DANISH METEOROLOGICAL INSTITUTE

TECHNICAL REPORT

03-13

Implementation of QuikScat SeaWinds data in the EUMETSAT Ocean & Sea Ice ice product

January 2003

Rasmus Tonboe
Jörg Haarpaintner

ISSN 0906-897X
ISBN

Copenhagen 2003

Preface

The european organisation for the exploitation for meteorological satellites (EUMETSAT) Ocean and sea ice satellite application facility project (O&SI SAF) now entering the operational phase is daily issuing a data fusion sea ice product (O&SI SAF ice product). The statistical Bayesian data fusion method is used combining microwave radiometer data, visual/infrared and microwave scatterometer data. The derived sea ice parameters are: ice cover concentration, ice type and ice edge. The pre-operational test products were based on DMSP SSM/I, NOAA AVHRR and ERS-2 scatterometer data. The ERS-2 scatterometer, however, went out of operation in February 2001 and ASCAT the next European scatterometer will not be in operation till 2005. In order to close the gap between European scatterometer missions and include the important scatterometer data, it has been decided to introduce data from the American QuikScat mission. This report presents typical backscatter signatures for different ice chart classes by co-locating ice charts and QuikScat scatterometer data. These data are necessary before the operational implementation into the O&SI SAF ice product.

This report presents the work that has been done during the visit of Jörg Haarpaintner to DMI, Copenhagen, in the period 6-31 January 2003 and to MET.NO, Oslo, in the period 1-14 February 2003.

This work was made possible by the SAF visiting scientist programme financing Jörg Haarpaintner's (JH) visit to DMI and MET.NO. JH is financially supported by the UCAR visiting scientist programme to work at the National Ice Center, Washington DC.

During JH visit to DMI Lars-Anders Breivik and Harald Schyberg from MET.NO visited DMI the 22nd of January 2003 to discuss the operational implementation of the results and JH work during the two upcoming weeks at MET.NO.

Keywords: SeaWinds sea ice parameter statistics, sea ice parameter variability, O&SI SAF operational data fusion ice product, Greenland.

List of contents

1.	Introduction	3
2.	Instrument and Data	5
2.1	SeaWinds instrument	5
2.2	SeaWinds data	5
2.3	Greenland ice charts and conventions	6
2.4	Ku-band signatures for sea ice and ocean	7
2.5	O&SI SAF ice class definition	8
3.	Co-location method	10
4.	Results	11
4.1	Ice type discrimination into 4 categories	11
4.2	CERSAT daily standard deviation of the backscatter	13
4.3	Ice type discrimination into 6 categories	15
4.4	CERSAT standard deviation of the backscatter	16
4.5	Ice - water discrimination	18
4.6	Kolmogorov-Smirnov test	21
5.	Supervised Bayes classification	22
5.1	Ice-water discrimination	22
5.2	Calculation of probabilities for ice classification	22
5.3	Classification results	23
6.	Implementation into the EUMETSAT O&SI SAF ice product	25
6.1	Software and algorithm development in the processing chain	25
6.1.1	Reading the BUFR data	25
6.1.2	Computation of derived parameters	25
6.1.3	Open water threshold and Bayesian classification	26
6.1.4	Visualisation	27
6.2	Choice of parameters and statistics	27
6.3	Results on day 42 year 2003	27
7.	Discussion	30
7.1	Greenland ice charts	30
7.2	SeaWinds scatterometer data	30
7.3	Ice-open water discrimination	31
7.4	Ice type discrimination	31
7.5	Synergy with other satellite data	32
8.	Conclusions	33
9.	References	35
10.	Appendix	36

1. Introduction

Data fusion is a way of combining information in e.g. automated sea ice monitoring. The current O&SI SAF ice product is a data fusion project where radiometer (DMSP SSM/I) visual/infrared scanner (NOAA AVHRR) and scatterometers (ERS-2 AMI) data are combined using Bayes method for sea ice classification. The QuikScat SeaWinds scatterometer (QS) is well suited for operational sea ice monitoring (Long and Drinkwater, 1999) because of the: 1) the backscatter measurements of the earth surface are independent of daylight and cloud cover, 2) QS has complete daily coverage at high latitudes (>55°), 3) there is effective backscatter separation between ice types (Ezraty and Cavanie, 1999; Remund and Long, 1999), 4) there are distinct signatures for ice and water surfaces, and 5) the next SeaWinds scatterometer has been launched (Dec. 2002 on ADEOS II) to ensure mission continuity. The scatterometer information is in particular useful for ice type and ice water discrimination.

Ice cover is an indicative parameter for climate change. The total extent of the ice cover and the extent of the thick multi-year ice are important climate parameters. Investigations of the Arctic sea ice cover monitored by microwave radiometers the last 30 years show a decreasing trend correlated to global warming (Johannesen et al. 1999).

Sea ice is also an important parameter for the ocean – atmosphere heat exchange and information on ice cover and ice thickness should be included in numerical weather prediction models operating at high latitudes. The ice thickness is actually not measured from satellites today but may roughly be inferred by knowing the ice type. The ice type can be measured by microwave sensors because of the different dielectric and scattering properties that affect the total brightness temperature or backscatter. For example first-year ice has a higher complex dielectric constant and lower air bubble content in the upper 0-20cm than multi-year ice which gives less scattering in the radiated or backscattered microwaves from first-year ice.

The Danish meteorological institute (DMI) and National Ice Center (NIC) are currently using SAR for operational mapping of sea ice for the safety of navigation. However, because of the modest spatial coverage with SAR (maximum swath width ~500km), mapping of any given region is irregular and often only partial. Scatterometers and radiometers with wide swath widths (SeaWinds 1800km and SSM/I 1400km) have the potential to fill in the gaps between the SAR scenes, thus aiding the manual interpretation of the situation.

The purpose of the present report is to suggest SeaWinds parameters which are useful for operational and automated sea ice monitoring in O&SI SAF. The aim is to establish statistical values for selected ice classes and implement the SeaWinds data in combination with the already operational DMSP-SSM/I radiometer data. The statistical SeaWinds-sea ice data base is produced by co-location of SeaWinds data and DMI ice charts around Greenland.

In Section 2 the Seawinds scatterometer instrument and the ice chart data and conventions are presented. In section 3 we describe the co-location method and extraction of the SeaWinds statistical mean and standard deviation values for different ice classes. Section 4

presents the results, giving the typical monthly mean values of backscatter, polarisation ratio and standard deviation that can be used in the O&SI SAF ice classification. Section 5 presents Bayesian classification and classification results using *Centre ERS d'Archivage et de Traitement* (CERSAT) data. Section 6 presents the operational implementation in the O&SI SAF processing chain and first results of an operation simulation. In section 7 we discuss the SeaWinds sea ice parameters and their physical variability. Section 8, the conclusions, sums up the recommendations. The Appendix contains the complete 2-year co-location statistics.

2. Instrument and Data

In this section the QuikSCAT SeaWinds instrument is presented together with the QS data and the DMI ice charts. Further, typical SeaWinds signatures for different ice types and the O&SI SAF ice class definitions are described.

2.1 SeaWinds instrument

The SeaWinds instrument onboard the QuikScat satellite is a Ku-band pencil beam scatterometer using a rotating dish antenna with two spot beams that sweep in a circular pattern. Its operating frequency is 13.4 GHz. The outer beam is transmitting and receiving at vertical polarisation (VV) with an incidence angle of 55° . The inner beam is transmitting and receiving at horizontal polarisation (HH) with an incidence angle of 47° . The swath width of the outer beam is 1800 km and the inner beam 1400km (Leidner et al. 2000). At high latitudes (>55°) the daily coverage is complete for both polarizations.

The QuikScat SeaWinds fact box in table 2.1 summarizes the instrument parameters (Leidner et al. 2000).

Launch date: June 1999	Geo-location accuracy ~1km
Altitude over equator: 803km	Type: scanning pencil beam
Inclination 96.6°	Sun-synchronous orbit 6am/pm local time
Repeat cycle: 4 days	Swath width: • VV (outer beam) 1800km • HH (inner beam) 1400km
EM frequency: Ku-band 13.4GHz	Incidence angle: • 55° (VV) • 47° (HH)

Table 2.1.: QuikScat – SeaWinds fact box.

2.2 SeaWinds data

The measurement geometry, polarization and frequency gives at least 4 parameters which are interesting for sea ice classification: 1) The backscatter coefficient at HH and 2) VV 3) the polarization ratio defined as the ratio of the difference over the sum of the backscatter at HH and VV and 4) the anisotropy defined as the difference between fore and aft measurements. When the swath data are gridded in e.g. a daily product the daily backscatter variation within the grid cell is also a useful parameter. This is called the daily standard deviation of the backscatter. The anisotropy is included in the daily standard deviation of the backscatter that we use in this study.

The QuikScat SeaWinds L2B near real time BUFR data product is distributed by NOAA NESDIS. The data are available ~3 hours after the satellite overpass (Tonboe and Ezraty, 2002).

The backscatter coefficient is a composite of backscatter values from several pulses. Each pulse footprint is divided in range into slices. If the centre of a slice falls within a 25 km x

25 km predefined wind cell it is assigned to this cell through an appropriate average. For the near-real-time product only slices from the first four pulses are used in order to reduce processing time at the satellite facility (Leidner et al. 2000).

2.3 Greenland ice charts and conventions

DMI is producing weekly ice charts covering the waters around Greenland. The classification of the ice in the ice chart is done manually using a synergy of satellite data e.g. Radarsat ScanSAR, NOAA-AVHRR and DMSP-SSM/I from one day. Radarsat ScanSAR coverage in Greenland waters is concentrated around the navigationally most important areas i.e. Tasiilaq, Cape Farewell and Disko Bay.

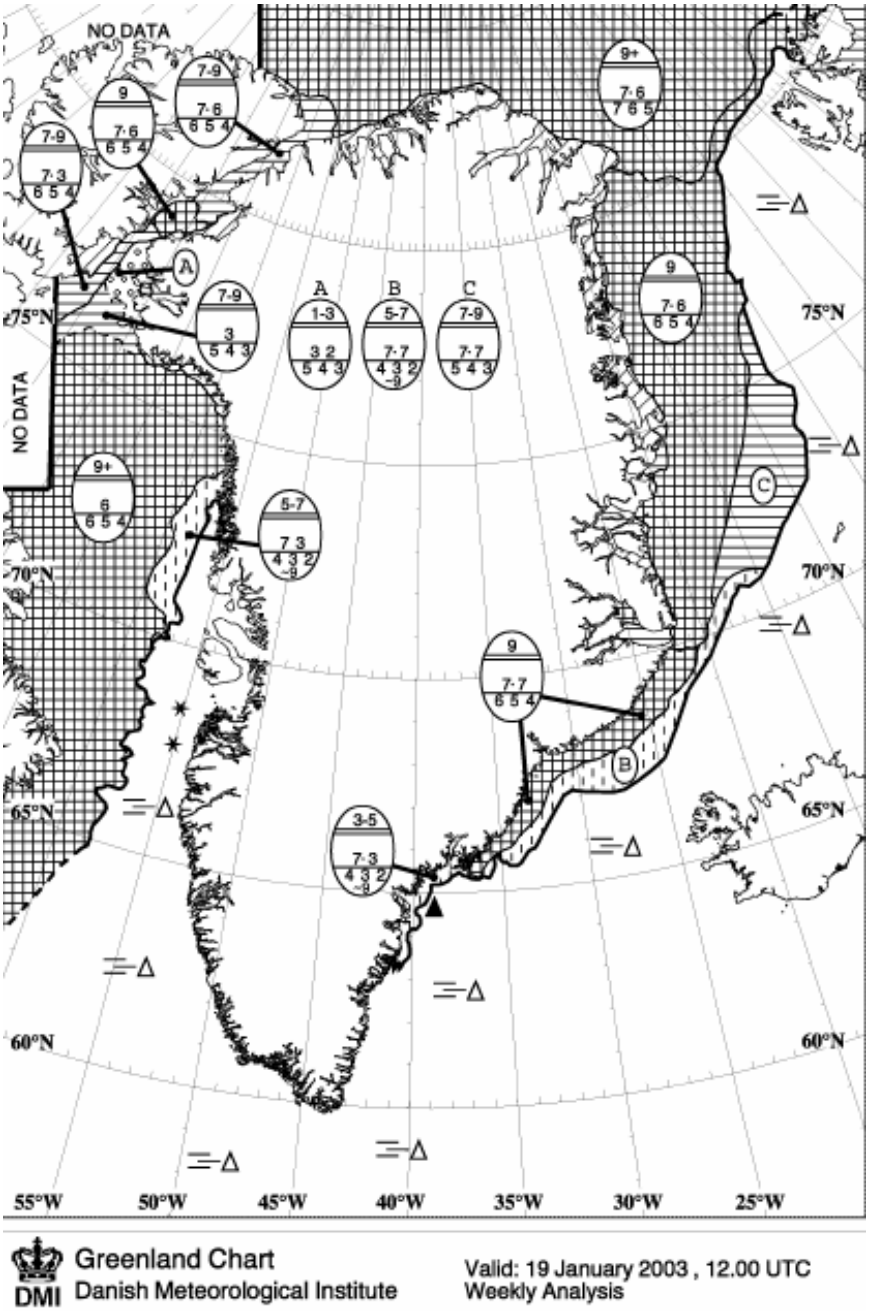

Figure 2.1: DMI ice chart of Greenland.

The sea ice drifting along the Greenland east coast consist in general of multi-year ice from the central Arctic, first-year ice formed along the Siberian coast and in leads, icebergs from the east Greenland Glaciers and new-ice formed in polynyas and along the ice edge. The ice analyst doing the manual interpretation of the ice chart does usually not have data which are useful for discriminating different ice types. The ice type information in the ice chart is therefore often an extrapolation of earlier (Radarsat) data or based on experience. The ice analyst will unless there is data to suggest otherwise classify the ice in the east Greenland current to contain fractions of multi-year ice. This should be noted because the backscatter statistics in the following are ordered according to the thickest sea ice type and this will on the east coast then normally be multi-year ice.

The **DMI ice charts** are classified according to the WMO 'egg code'. The classification code is summarised in table 2.2. The ice cover is characterised according to 4 parameters: 1) ice covered fraction or ice concentration, 2) ice thickness, 3) distribution of the ice, homogeneously or in belts, and 4) floe size.

Total ice concentration 0 is sea ice free, 1 is complete ice cover.
Concentration of the 3 thickest ice types
Class of 3 thickest ice types New ice Thin ice Young ice First year ice Old ice Second year ice Multi year ice Glacier ice
Concentration of belts (if any) **Floe size/type** Pancake ice Slush ice Growlers Small floes Medium floes Big floes Vast floes Ice fields Fast ice Glacier ice

Table 2.2: Egg code conventions.

2.4 Ku-band signatures for sea ice and ocean

The surface types are defined according to their scattering properties. **First-year ice** is saline ice with a large surface backscattering component. Typical SeaWinds backscatter for 100% FY ice during winter is –18 to -16dB. **Multi-year ice** is low-saline ice with high air bubble content. The backscatter is dominated by volume scattering. Typically volume

scattering results in uniform scattering where the drop-off in backscatter with incidence angle is small. SeaWinds backscattering coefficients for 100% MY ice is ~ –9 to -7dB. **Open water** backscatter is a function of surface wind and characterized by a large difference between HH and VV backscatter. It has a large drop-off in backscatter with incidence angle compared to sea ice and the backscatter is anisotropic for different look angles. Open water backscatter is usually less than -12dB (-12dB is for upwind wind speed ~20m/s). Under calm wind conditions (<5m/s) ocean backscatter is below -23dB and lower than backscatter from most ice types.

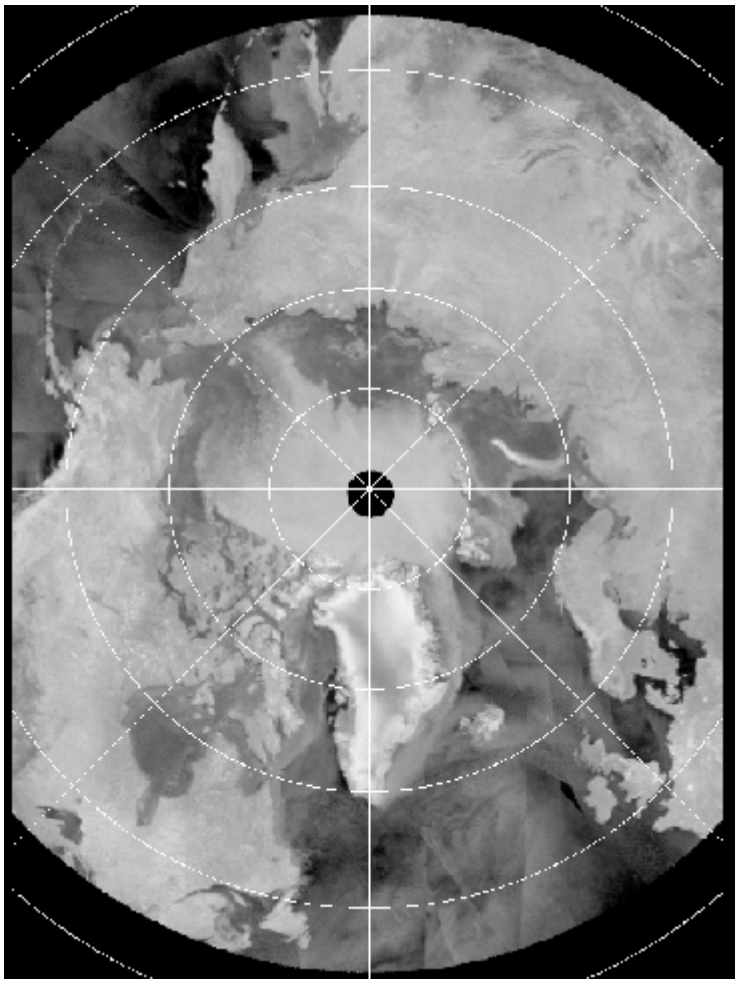

Figure 2.2: QuikSCAT SeaWinds backscatter of the Arctic sea ice January 23rd 2003 (©Brigham Young University & National Ice Center).

2.5 O&SI SAF ice class definition

The current **O&SI SAF classification code** for ERS scatterometer data is operating with different ice concentration categories and two different ice types. 'Open ice' is defined as 40-60% ice cover. 'Close ice' is defined as 70-90% ice cover. The ice types are defined in areas with 100% first-year ice and 100% multi-year ice. This definition is inconsistent with the scattering characteristics of the ice classes defined in the ice chart and failed to define the low concentration ice. It has therefore been modified. As a first try we defined 4 categories: 1) open FY ice, FY<70%, 2) close FY ice, FY>70%, 3) open MY ice, MY<70%,

and 4) close MY ice, MY>70%. In order to investigate the separation between the medium and open ice better 6 categories were defined: open, medium and close concentration for both, FYI and MYI. This modified definition gives better contrast in QS data. An ice class is defined as a MYI class for any partial MYI concentration. The ice type is FYI only if no MYI at all is present. Open, medium and close classes refer to the total ice concentration, 0 - 30%, 30 -70%, 70 - 100%, respectively.

3. Co-location method

The ice charts are gridded in a 10km regular grid. This grid is used for the co-location of the QS L2B data. Each grid point contains information extracted from the WMO egg code: 1) total ice concentration, 2) thickest ice type, 3) second thickest ice type and 4) largest floe size. According to these characteristics, the 6 ice classes are defined by ice type, i.e. MY ice or FY ice, and total ice concentration (in tenth), i.e. close (7-10), medium (3-7), open (0-3). Because these satellite data have lower resolution than the ice chart grid, all grid points in the ice chart which are a neighbour to a different ice class are excluded in the co-location. With a co-location radius from centre to centre of maximum 8km this ensures that most of a satellite data pixel should be within a certain ice area when assigned to that area, i.e. the method is collecting all SeaWinds data within a certain ice type area. Figure 3.1 presents an example situation, showing which grid points are used or not in the co-location if points are neighbour to surface type boundaries.

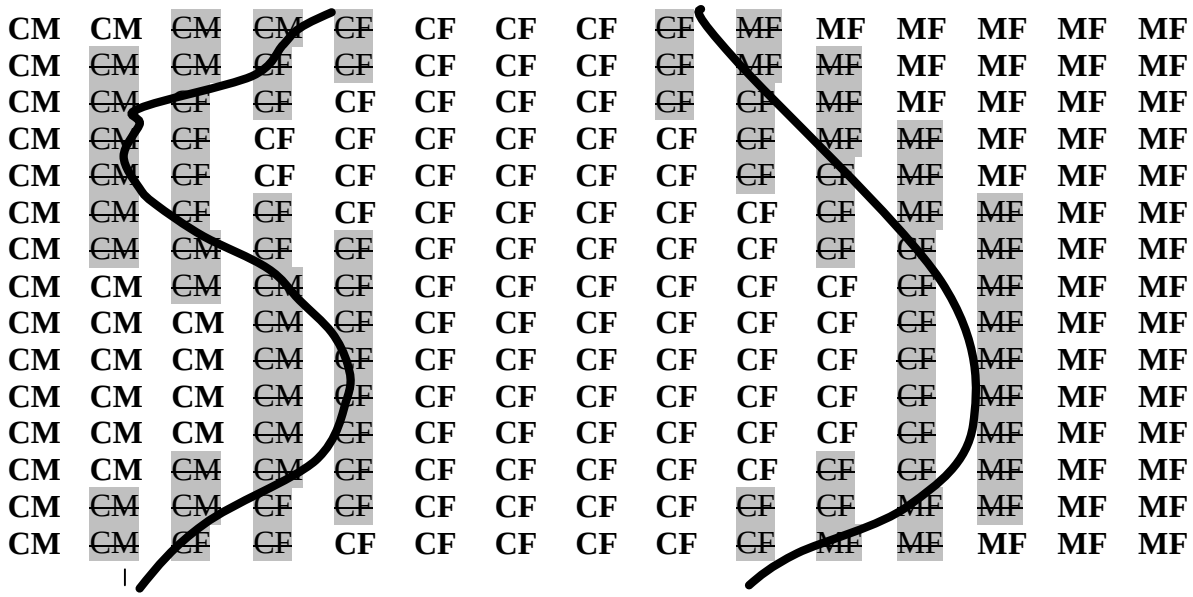

Figure 3.1: Usage of grid point data in the case of ice type boundaries. Bold grid points are used for establishing the statistics. Grid points in grey are discarded. The bold lines represent ice type boundaries. CM, CF and MF abbreviate the ice classes, close MYI, close FYI and medium FYI, respectively.

By co-location, the monthly mean and standard deviation HH and VV backscatter and polarization ratio are computed for each ice class. The statistical parameters are an average over the entire Greenland region covered by the ice chart. The L2B data are not gridded during the co-location process. Therefore it is not possible to extract the daily standard deviation for each ice chart grid point. Instead of gridding the L2B data we use the CERSAT gridded ice products which are available online on the internet. These data are co-located to the ice charts to retrieve the daily standard deviation of the backscatter.

4. Results

The Greenland ice charts during a two year period (October 2000 to September 2002) are co-located with the L2B data and CERSAT data. Each ice chart is valid for one day and only scatterometer data the same day are used in the co-location. The co-location yields typical mean backscatter signatures for the different ice chart classes throughout the season. Monthly mean backscatter values, the polarization ratio and the daily standard deviation of the horizontal and vertical backscatter are presented graphically in the following. The exact statistical values are given in the appendix.

4.1 Ice type discrimination into 4 categories

First-try with 4 ice classes to separate between close (70%-100%) and open (0%-70%) MY and FY ice. The exact statistical values for each class and all parameters are given in Appendix table A.

Figure 4.1 presents the mean 2-year monthly average backscatter values, s_{0HH} and s_{0VV}, in dB of each ice class.

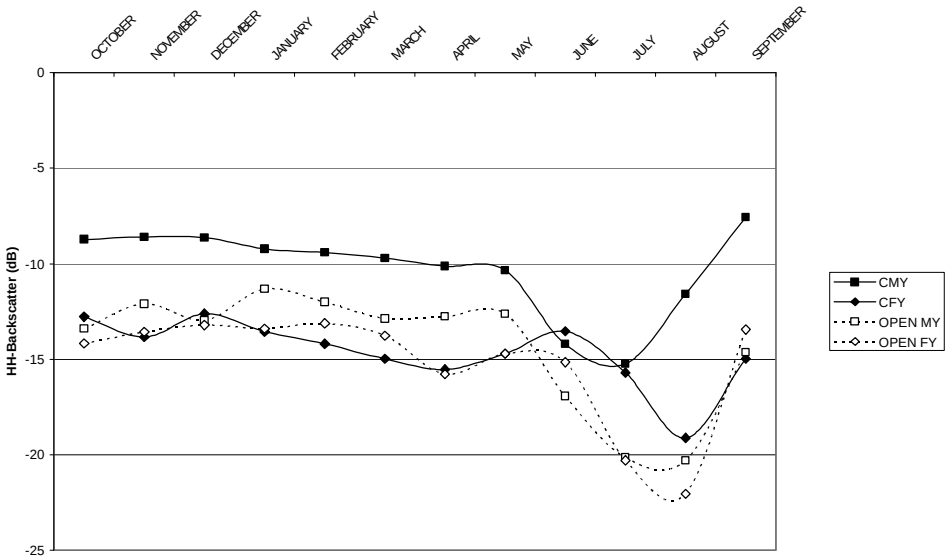

a)

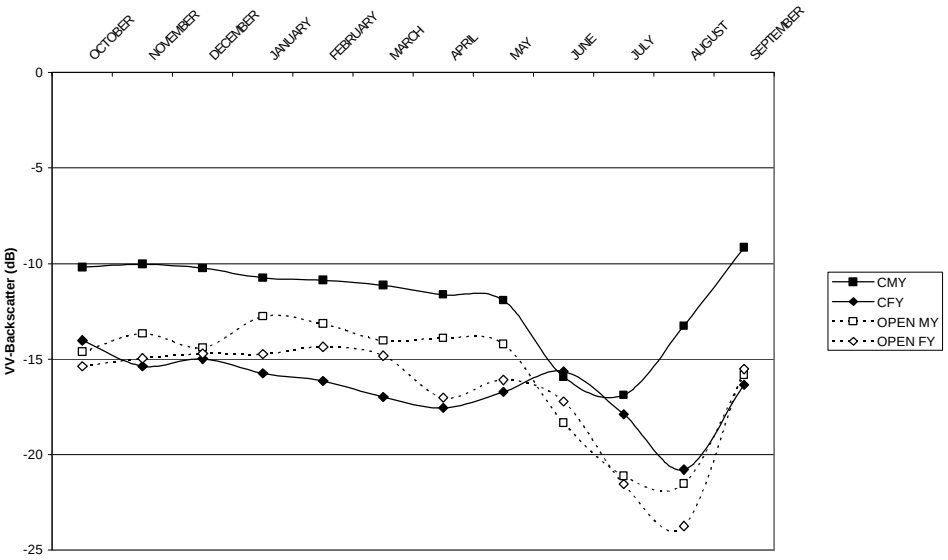

b)

Figure 4.1: Monthly mean backscatter values for each ice class in horizontal (a) and vertical (b) polarization. CMY – close multi-year ice, CFY – close first-year ice, open MY – open multi-year ice, open FY – open first-year ice.

The seasonal evolution of the backscatter for the vertical and the horizontal polarization are similar only s_{0HH} being ~ 2.5 dB higher than s_{0VV}.

During the winter months (September – May) there is a net separation between **close MYI** and the other ice classes. This makes close MYI a distinct backscatter class with s_{0HH} values in the range of (- 10.5 dB- -7.5 dB).

During late winter (January – April) mean backscatter for **open MYI** is higher than open and close FYI backscatter. The mean backscatter of FY and MY ice can be separated by a threshold of –13 dB.

Close and open FYI are in the same range of backscatter during the year. Earlier studies by Tonboe (2001) of the FYI backscatter as a function of ice concentration show that backscatter values do not increase uniformly with ice concentration but has a maximum backscatter at medium ice concentrations around 70%.

Ice type classification using backscatter is difficult during the **summer** months (June - August) when there is ice surface melting.

Figure 4.2 presents the mean of the polarization ratio for each month.

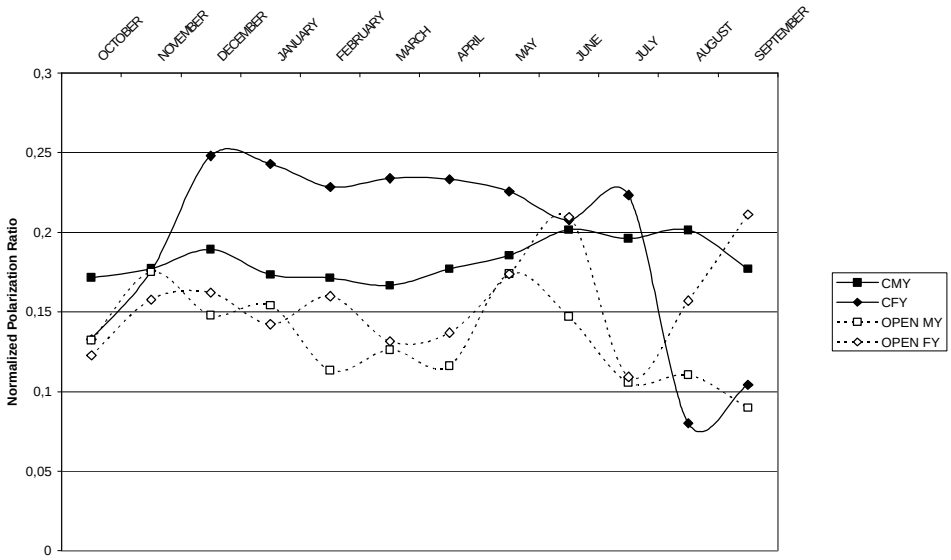

Figure 4.2: Monthly mean normalized polarization ratio for each ice class.

Effective discrimination between ice types is only possible in winter when the surface properties affecting the backscatter are stable. During winter, high ice concentrations have higher polarization ratios than low ice concentration areas for both FYI and MYI ice types. The close FYI class has the highest polarization ratio from December to July with mean values between 0.21 and 0.25. The polarization ratio of close MYI is stable during the cold season between 0.17 and 0.20. Low FY- and MY ice concentrations have polarisation ratio values between 0.1 and 0.17, except open FYI during summer (0.12-0.22). During winter the polarization ratio is a useful parameter to separate close ice from open ice.

4.2 CERSAT daily standard deviation of the backscatter

Figure 4.3 shows the seasonal evolution of the CERSAT standard deviation for the different ice classes. The standard deviation of the vertically and horizontally polarized backscatter is similar. The standard deviation of the backscatter seems uncorrelated to ice type, i.e. the standard deviation is nearly the same for both, FYI and MYI. The daily standard deviation of the backscatter is however related to ice concentration. Low concentration ice has higher daily standard deviation of the backscatter than high concentration ice cover.

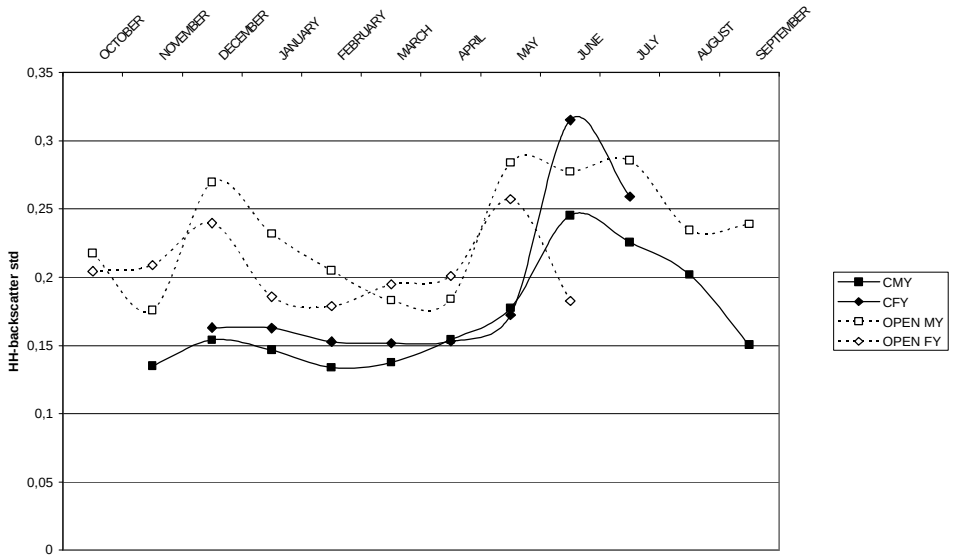

(a)

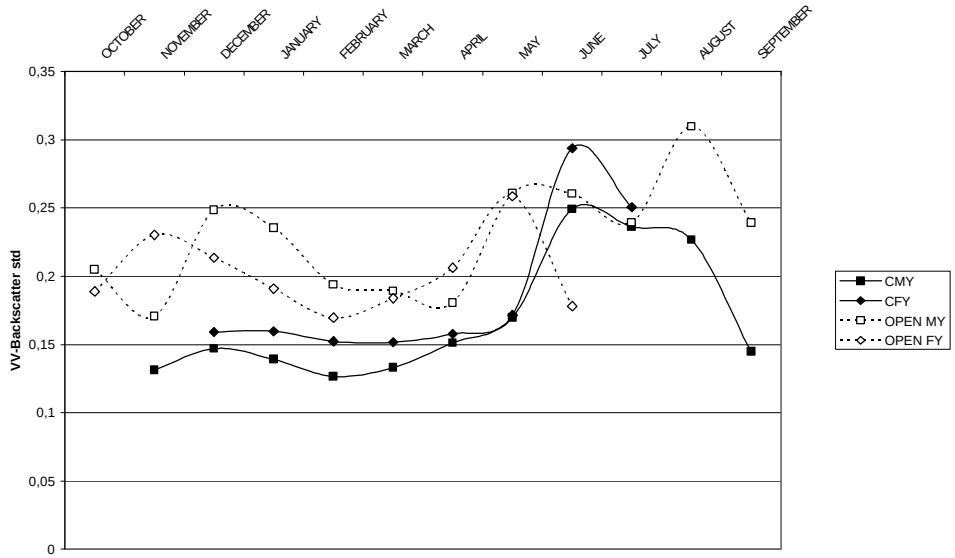

(b)

Figure 4.3: Monthly mean standard deviation for horizontal (a) and vertical (b) polarization extracted from the gridded CERSAT data.

4.3 Ice type discrimination into 6 categories

The ice type classification into four classes was successful. However the open ice classes include a wide range of ice concentrations (0-70%). Therefore we sub-divided the ice cover into six classes which are:

- close MYI (CMY), with ice concentrations higher than 70%,
- close FYI (CFY), with ice concentrations higher than 70%,
- medium MYI (MMY), with ice concentrations from 30% to 70%,
- medium FYI (MFY), with ice concentrations from 30% to 70%,
- open MYI (OMY), with ice concentrations less than 30%, and
- open FYI (OFY), with ice concentrations less than 30%.

Figure 4.4 presents the mean two-year monthly average backscatter values, s_{0HH} and s_{0VV}, in dB of each ice class.

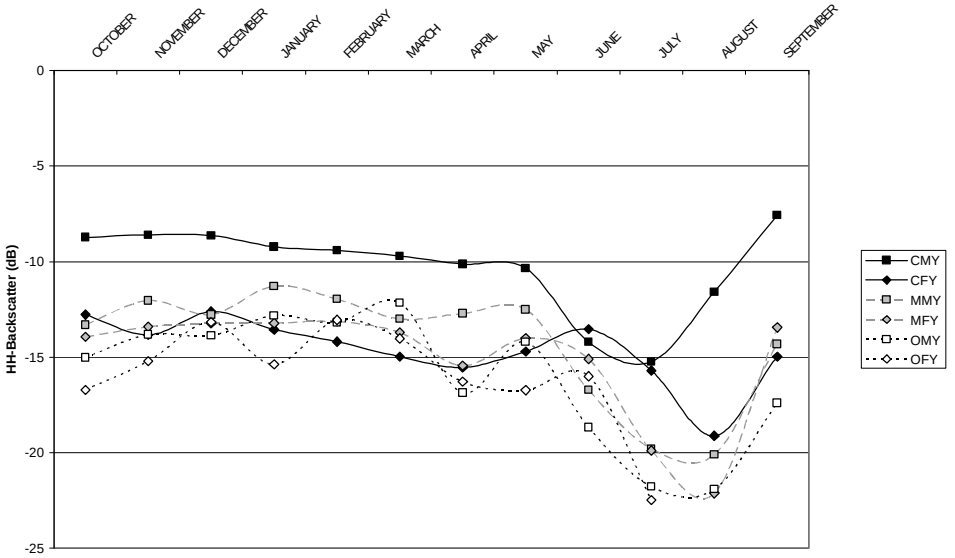

(a)

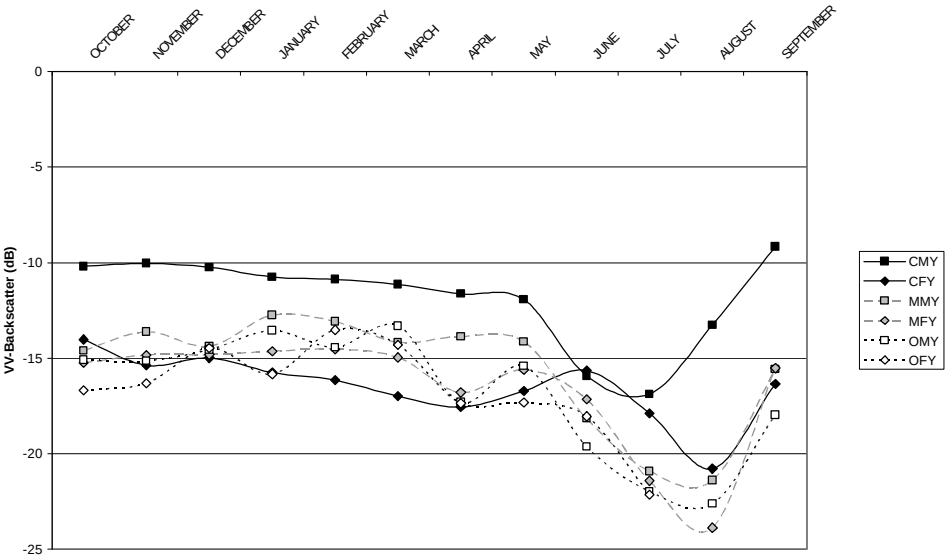

(b)

Figure 4.4: Monthly mean backscatter values for the 6 ice class in horizontal (a) and vertical (b) polarization.

The seasonal evolution of the backscatter for the vertical and the horizontal polarization are similar, only s_{0HH} being ~2.5 dB higher than s_{0VV}.

During winter, high concentration MYI is separated from the other classes with s_{0HH} in the range of -10.5- -7.5 dB. As with the 4 classes a threshold of -13dB can separate the MYI and FYI backscatter mean during winter. The other classes mean backscatter overlap. FYI, medium, low concentration MYI and ocean backscatter signatures are in the same range backscatter. The standard deviation of the backscatter is in the range of 30% to 50% during winter for close and medium classes, and typically 50% to 100% during summer and for open ice classes.

Figure 4.5 presents the seasonal evolution of the mean polarisation ratio for each ice class.

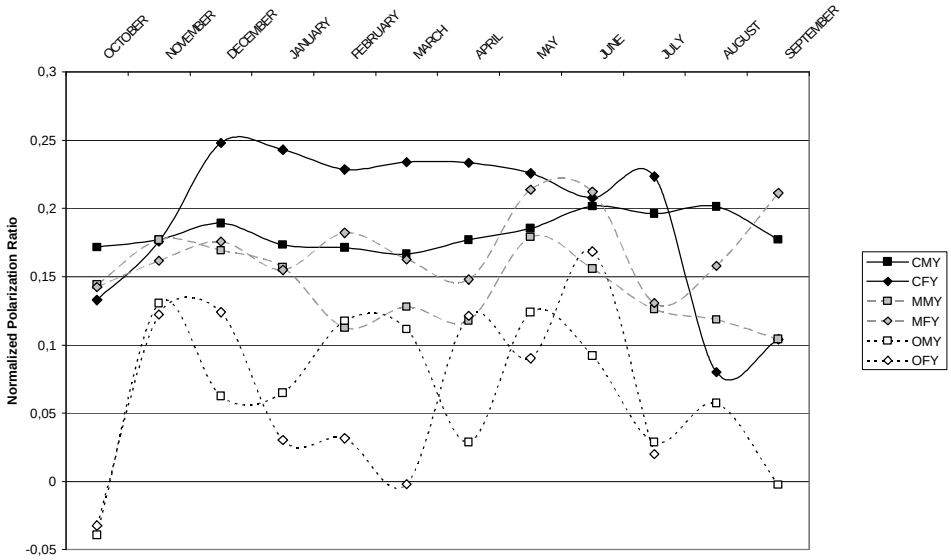

Figure 4.5: Monthly mean polarization ratio for the six ice classes.

The polarisation ratio for both FYI and MYI is larger for higher ice cover concentrations. High and medium concentration ice types can be separated by the polarisation ratio mean. Low ice concentration ice types can not been separate by type.

4.4 CERSAT standard deviation of the backscatter

Figures 4.6 show the seasonal evolution of the CERSAT standard deviation of the backscatter of different ice classes. The standard deviation of the backscatter is similar in both vertical and horizontal polarization and it is nearly equal for both FYI and MYI. The standard deviation is related to the ice concentration. For open ice the standard deviation is higher than for close ice. The co-location of the gridded CERSAT data and the ice charts did not yield enough values for reliable statistics in the open ice classes (< 30% ice concentration).

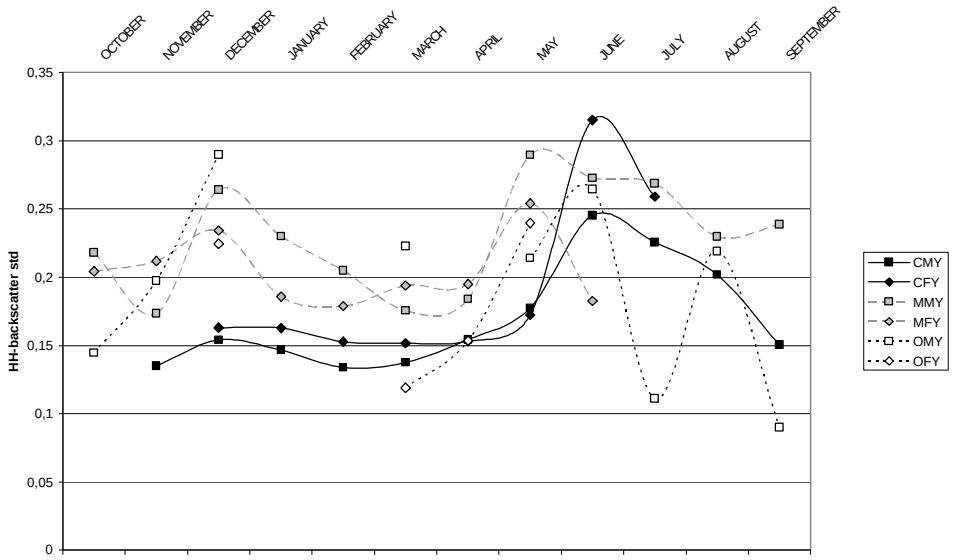

(a)

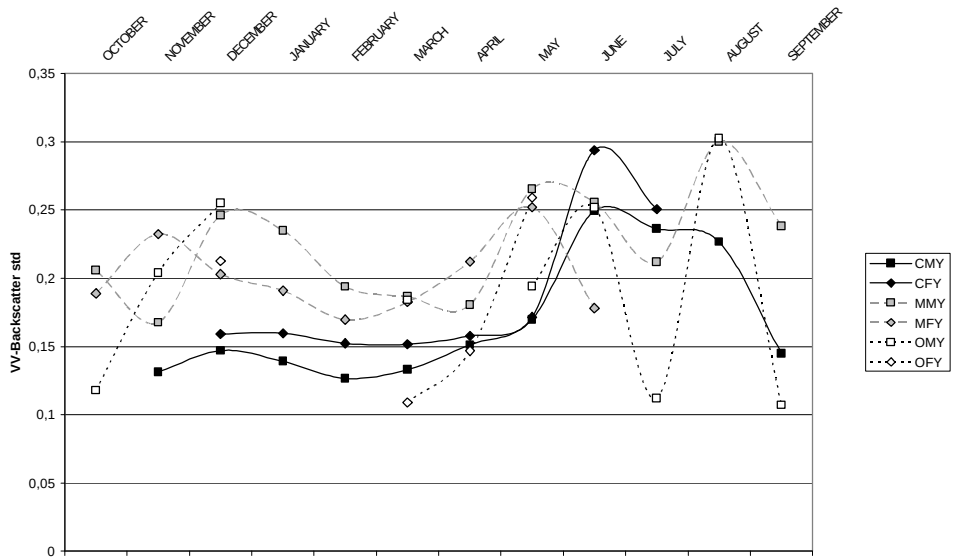

(b)

Figures 4.6: Monthly mean standard deviation for horizontal (a) and vertical (b) polarization extracted from the gridded CERSAT data.

The exact statistical values for each class and all parameters are given in Appendix Table B.

4.5 Ice - water discrimination

Two parameters may be used to discriminate between water and ice: 1) the normalised standard deviation of the daily backscatter, and 2) the polarisation ratio. These two parameters are describing distinct differences in backscatter processes from sea ice and ocean surface influenced by surface wind. The QS polarisation ratio is a function of the polarisation difference in HH and VV backscatter and the decline in backscatter with incidence angle. The standard deviation of the backscatter is a function of: the backscatter difference between fore and aft measurements, the geophysical variation and the processing and instrumental noise. The QS polarisation difference between the HH and VV polarised backscatter from ice is in general positive (HH>VV) and over open water it is negative (HH<VV). The difference between fore and aft backscatter measurements in QS over open water is dependent on the wind direction and the position across swath, i.e. some wind cells will have large difference between fore and aft while others will have nearly none. However since the backscatter over open water is anisotropic there is normally a difference between fore and aft measurements. The backscatter from ice is isotropic and does not depend on the radar look direction. The backscatter variations due to changes in the geophysical conditions are also larger over water than over ice for a given period e.g. one day. Because of the anisotropic backscattering and rapid geophysical variability, i.e. the standard deviation, over open water is larger than for ice. The backscatter over open water can be modelled using backscatter/wind models e.g. the model described by Wentz and Smith (1999). The results presented in Figures 4.7 to 4.9 correspond to the predictions of this model. The ocean backscatter was divided into wind speed bins and the mean backscatter for each bin presented together with the 6 ice classes.

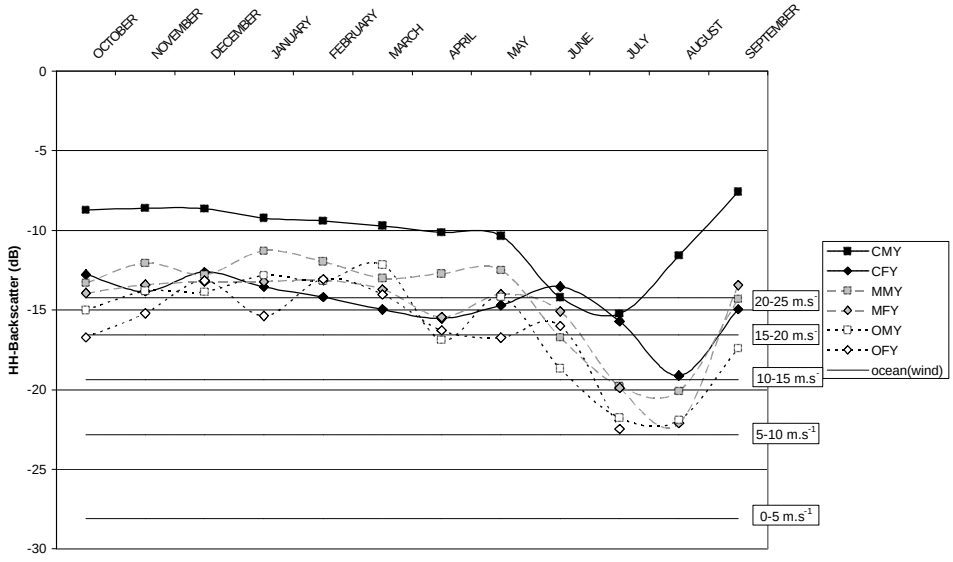

(a)

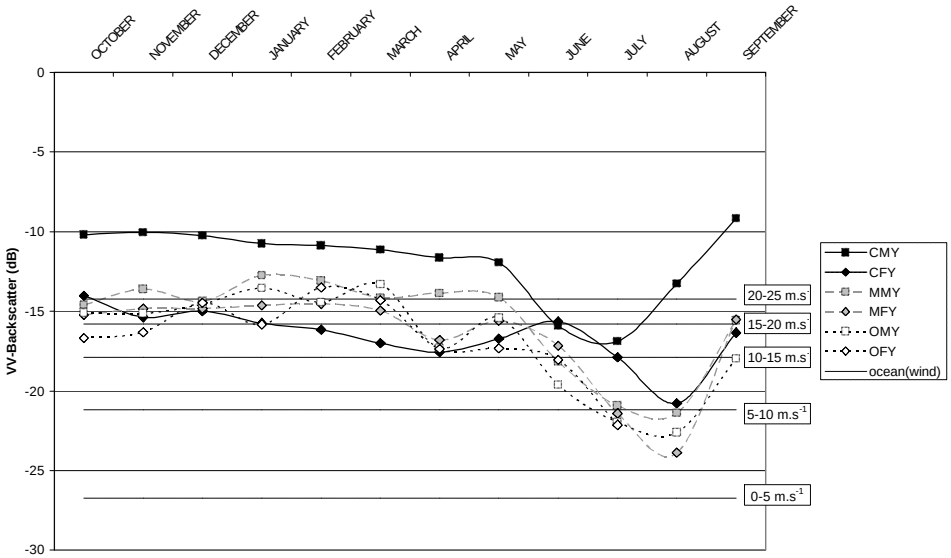

(b)

Figure 4.7: Comparison between backscatter over open water and over ice in horizontal (a) and vertical (b) polarization.

It is possible, during winter and calm wind conditions, to discriminate ice from open water using backscatter. For example wind speeds below 5m/s give backscatter below -23dB which is lower than most ice backscatter. In summer (June – August) ice surface melt may lower the mean ice backscatter to -25- -20dB. A winter threshold between open water and ice could be ~ -23 dB. In summer when discrimination using backscatter alone is difficult, a threshold below -25 dB should be used.

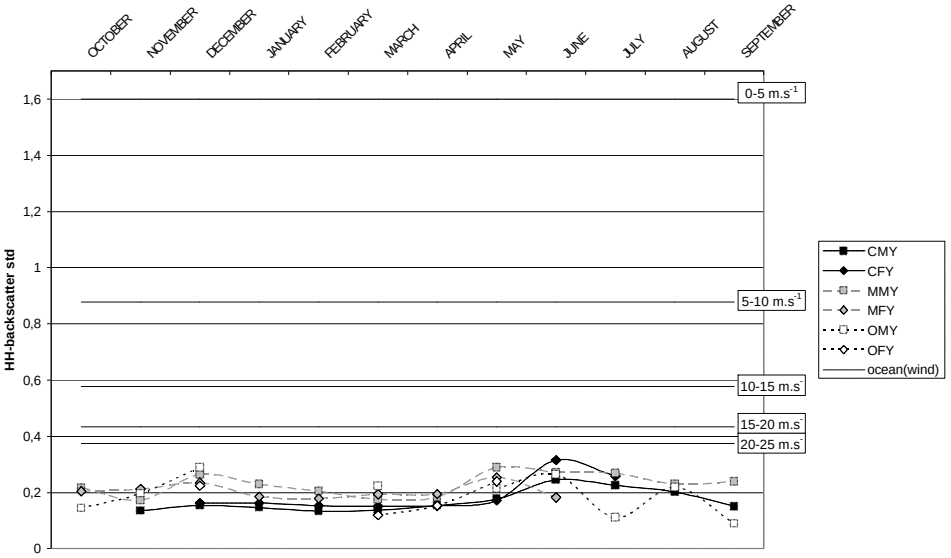

(a)

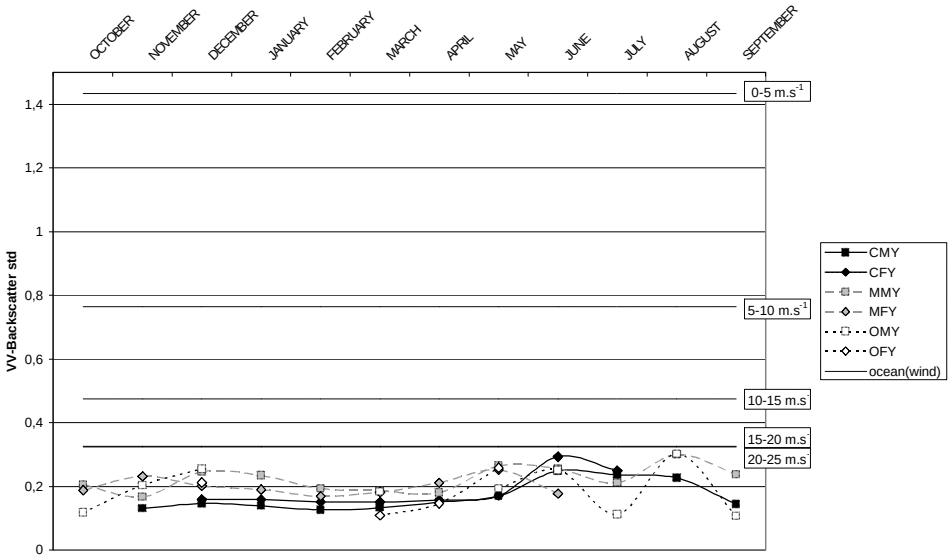

(b)

Figure 4.8: Daily standard deviation per pixel location for open water and ice in horizontal (a) and vertical (b) polarization.

Figure 4.8 shows the daily standard deviation for ice pixels and average anisotropy over the open water, i.e. variability for each ice class and wind speed. It is clear that the variability over open water is higher than that over ice.

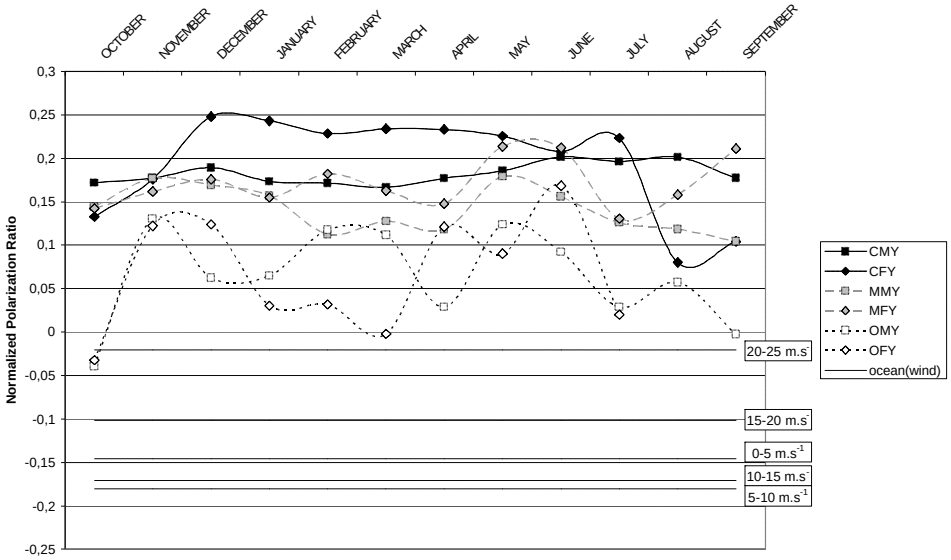

Figure 4.9: The polarization ratio for the 6 ice classes and open water signature of 5 wind speed bins: 0-5 m/s, 5-10 m/s, 10-15 m/s, 15-20 m/s, 20-25 m/s.

Figure 4.9 shows the positive polarization ratio over ice covered areas compared to a negative polarization ratio over open water.

4.6 Kolmogorov-Smirnov test

The hypothesis of the QS parameters distribution being Gaussian for each ice type class is tested using a Kolmogorov-Smirnov test. The test probability threshold is 5%. All parameters and all ice classes are tested using this test. For the compiled 2 year classes, presented above, none of the parameters or ice classes are Gaussian.

5. Supervised Bayes classification

The following section is reviewing the Bayes classification for satellite data and tuning the classification method using an example. As an example, the ice class statistics given in this report were used to classify a CERSAT backscatter map covering the Arctic on March 18th 2002.

5.1 Ice-water discrimination

First ocean and sea ice pixels are separated by thresholds, using the three parameters: 1) HH-backscatter, 2) polarization ratio, and 3) the normalized standard deviation.

A pixel is considered as open ocean if:

the HH-backscatter s_{HH} < -25 dB,
OR the polarization ration PR < -0.02
OR the daily standard deviation > 0.4

The thresholds are set at a level where even low concentration ice should be detected. However, using these thresholds ocean pixels are erroneously classified as ice in areas inflected by high surface winds (>15m/s). Additional data or filtering can possibly eliminate misclassified ice pixels. However in this example we focus on the ice type classification and the ice water discrimination should be refined in a future study.

5.2 Calculation of probabilities for ice classification

Bayes formula (1) is used for ice type classification of ice pixels:

$$p(C_i|x_j) = \frac{p(C_i)p(x_j|C_i)}{\sum_k p(C_k)p(x_j|C_k)} \qquad (1)$$

where
$p(C_i|x_j)$ is the probability of getting the ice class C_i given the value x_j for parameter j,
$p(C_i)$ is the probability of getting the ice class C_i,
$p(x_j|C_i)$ is the probability of getting the value xj for parameter j, given the ice class C_i.

The probability distribution, i.e. distribution function f, is assumed to be Gaussian according to formula 2:

$$f(x_j; \overline{x_j}; s^2) = \frac{1}{\sqrt{2ps^2}} e^{\frac{-(x_j-\overline{x_j})^2}{2s^2}} \qquad (2)$$

where $\overline{x_j}$ is the mean value of x_j and s^2 is the variance of x_j.
The different parameters are considered independently, so that the total probability P of getting the ice class C_i given all the values x_k is the product of all $p(C_i|x_j)$, i.e.

$$P(C_i|x_k) = \prod_k p(C_i|x_k) \qquad (3).$$

The class with the highest probability is selected.

5.3 Classification results

The supervised Baysian classification is using the mean and variance of QS ice class parameters for computing the probability of different surface types using equation 2. Here 4 QS parameters are used to classify 6 different ice type classes. The QS parameters are: 1) HH backscatter, 2) VV backscatter, 3) polarisation ratio, and 4) normalised daily standard deviation. The 6 ice types are described in section 4.2.

Different configurations are tested. In figure 5.2a the 6 types are classified (a) using only the HH and VV backscatter and the polarisation ratio. In Figure 5.2b the daily standard deviation is included in the classification. The Gaussian distribution function for the HH-backscatter is shown in Figure 5.1a. Because of the large differences in the variance for each ice type, the probability functions of ice classes with a low variance dominate over ice classes with a high variance.

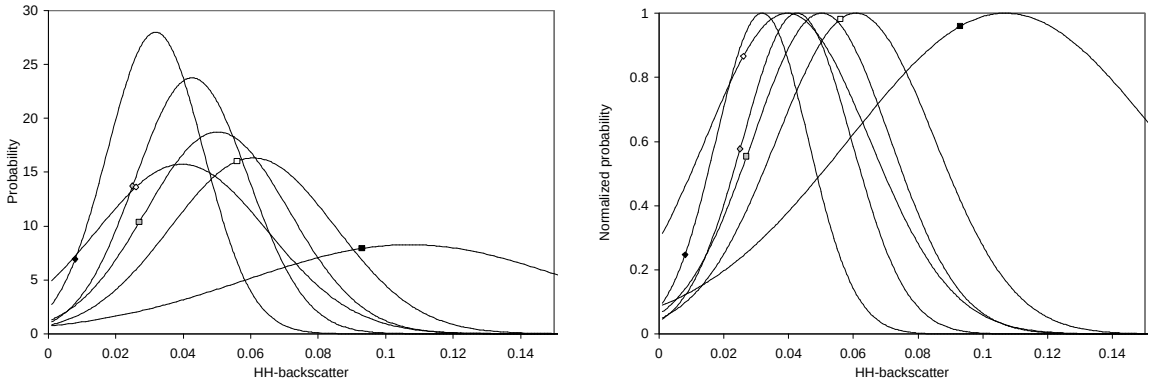

Figure 5.1: Probability distribution of the different ice classes for the HH-backscatter parameter (a) using the formula (2), and (b) normalized to 1.

The classification results in figure 5.2 show that the medium and low concentration types are probably assigned too high probabilities.

As a first try solution to this misclassification the distributions are normalised to 1 by dividing f with its maximum value $\frac{1}{\sqrt{2p\ \mathrm{var}}}$. The resulting probability distributions for HH-backscatter are shown in figure 5.1b. The classification is repeated in figure 5.3a using the normalized probability distributions without the daily standard deviation and figure 5.3b with the daily standard deviation of the backscatter. The 4 parameter combination with the normalised distributions gives the most satisfying results compared to general knowledge of the Arctic ice types.

The results in figure 5.3a and 5.3b with the normalised distributions give satisfying classification results. Separation between close FYI and close MYI is good. Pixels representing medium and low FYI and MYI concentration are present along the ice edge as

expected. Possible misclassifications were found in the central Arctic at the border between close FYI and close MYI along the Eurasian continental shelf. Some pixels are here erroneously classified to medium and low concentration classes and the classification in figure 5.3a assigns part of pixels in the Chukchi Sea to medium ice concentration. By including the daily standard deviation as a classification parameter changed those medium concentration pixels to close ice pixels, but also introduced more close and medium MYI in the Labrador Sea along the Canadian coast. A more rigorous validation is necessary in the future for the final selection of classification parameters and possible tuning of the classification probabilities.

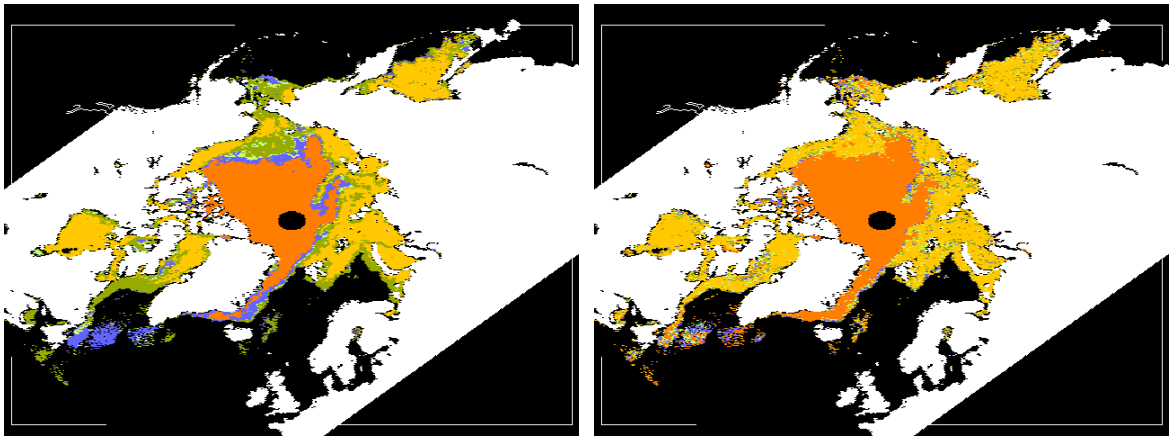

(a) (b)

Figure 5.2: Classification results March 18th 2002 using (a) HH, VV and polarization ratio (PR) and (b) HH, VV, PR and the daily standard deviation using the Gaussian probabilities with calculated variances. Color code: orange = CMY, yellow = CFY, light green = MMY, dark green = MFY, blue = OMY and grey =OFY.

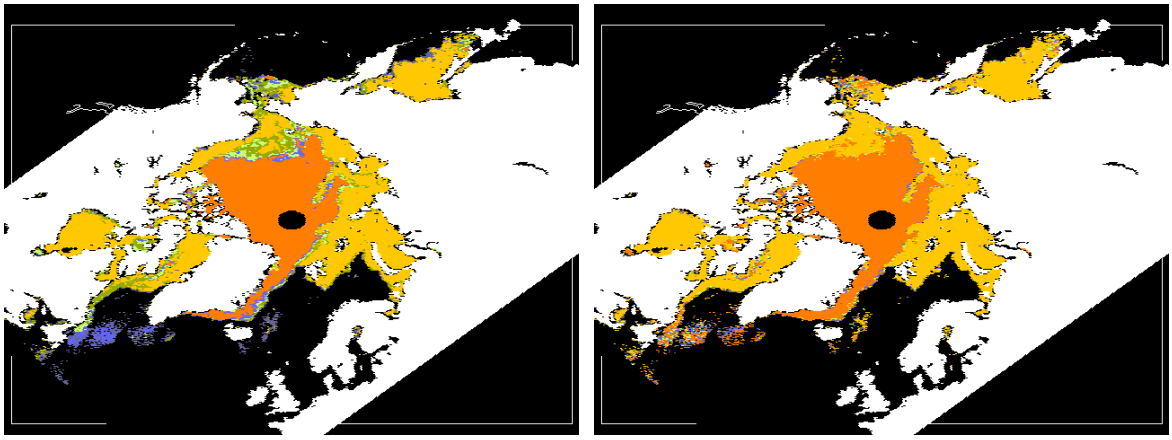

(c) (d)

Figure 5.3: Classification results March 18th 2002 using (a) HH, VV and polarization ratio (PR) and (b) HH, VV, PR and the daily standard deviation using the Gaussian probabilities with the normalized variances. Color code: orange = CMY, yellow = CFY, light green = MMY, dark green = MFY, blue = OMY and grey =OFY.

6. Implementation into the EUMETSAT O&SI SAF ice product

Jörg Haarpaintner's two week visit to MET.NO, was devoted the implementation of the sea ice backscatter signatures into the EUMETSAT O&SI SAF ice production chain. Due to the short time of the visit it was not possible to combine the classification results with SSMI, but a QS classification product was run in parallel with the SSMI product using the near-real-time QS L2B BUFR data. The results are presented in this section.

6.1 Software and algorithm development in the processing chain

The processing chain can be divided into 4 parts: 1) reading of the QS BUFR data and extraction of initial parameters, 2) computation of derived parameters and gridding into the O&SI grid, 3) Bayesian classification into the 6 ice classes and open water, including separation of ice and open water using additional parameters and 4) visualisation of the results.

Frank Tveter (part 1), Harald Schyberg (part 2 and 3) and Steinar Eastwood (part 4) from MET.NO, helped with the processing.

6.1.1 Reading the BUFR data

The L2B near-real-time BUFR data is decoded and the initial parameters are extracted. The L2B BUFR data contains fore and aft looking VV and HH measurements in each wind cell. These wind cells have a 25km pixel resolution. The data which is used for further processing are:

- the geographic position of the wind cell (longitude and latitude)
- the fore and aft HH and VV backscatter measurements
- the quality flag of the four backscatter measurements

The quality flag is used as a filter to omit uncertain measurements.

6.1.2 Computation of derived parameters

The four backscatter parameters: $s_{fore}(HH)$, $s_{aft}(HH)$, $s_{fore}(VV)$ and $s_{aft}(VV)$, are used to derive other parameters for each swath data pixel and the daily composite SAF grid data pixel.

For each individual swath pixel and composite SAF grid pixel the following is computed:

- mean horizontal and vertical backscatter values:
  $s_{0(HH)} = (s_{fore}(HH) + s_{aft}(HH))/2$,
  $s_{0(VV)} = (s_{fore}(VV) + s_{aft}(VV))/2$,
  and the daily mean
- polarisation ratio (PR) and the daily mean PR value for each pixel,
  $PR = (s_{0(HH)} - s_{0(HH)}) / (s_{0(HH)} + s_{0(HH)})$,
- HH and VV normalised anisotropies and the daily maximum of the two:
  $A(HH) = abs(s_{fore}(HH)-s_{aft}(HH)) / (s_{fore}(HH)+s_{aft}(HH))$
  $A(VV) = abs(s_{fore}(VV)-s_{aft}(VV)) / (s_{fore}(VV)+s_{aft}(VV))$
- daily maximum normalised cross-anisotropy,
  $A(HH,VV) = max(abs(s_{fore,aft}(HH)-s_{aft,fore}(VV)) / (s_{fore,aft}(HH)+s_{aft/fore}(VV)))$,

- daily standard deviation of each pixel in the SAF grid for both polarisations.
- daily maximum distance to 0 of the PR (PR_{Max}) in order to extract the measurements with the least ambiguity for separation between open water and sea ice.

All parameters are gridded into the EUMETSAT O&SI SAF grid.
Figure 6.1 shows the different parameters.

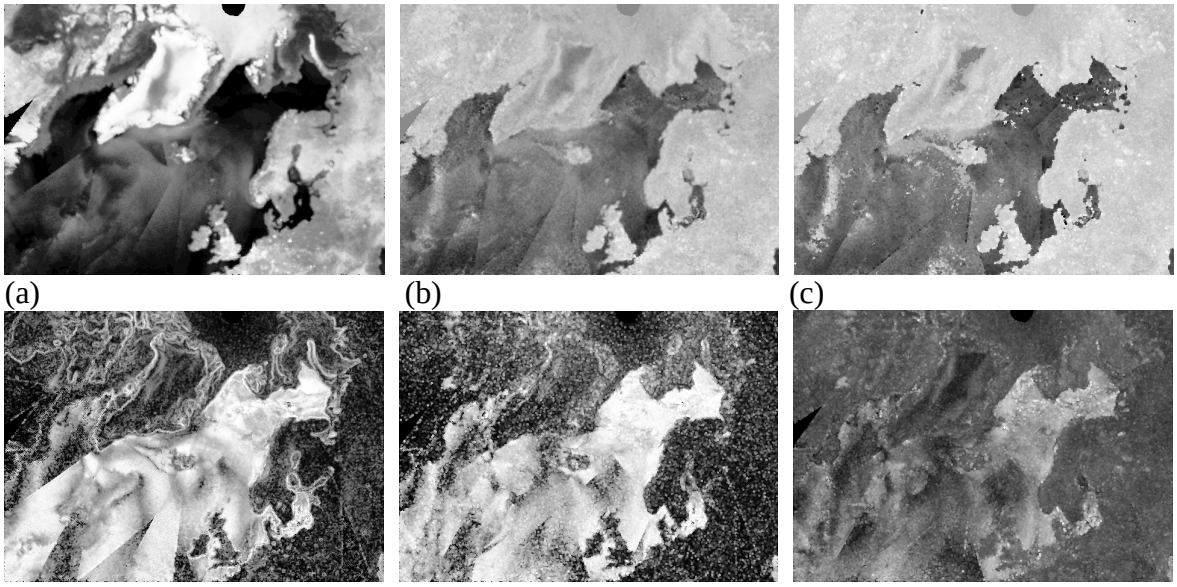

Figure 6.1: Images representing the following parameters: (a) $s_{0(HH)}$, (b) PR, (c) PR_{Max}, (d) daily standard deviation, (e) maximum anisotopy and (f) maximum cross-anisotropy.

6.1.3 Open water threshold and Bayesian classification

The classification process is divided into 2 parts: 1) threshold to eliminate most of the ocean pixels before the ice type classification, and 2) the Bayesian classification as described in section 5.

Most ocean pixels can be classified by thresholds using $s_{0(HH)}$, $s_{0(VV)}$, PR, PR_{Max} and the standard deviation. However, since the EUMETSAT O&SI SAF grid extends down to 50°N, several pixels at lower latitude only have a single measurement per day. It is therefore impossible to compute the daily standard deviation and the maximum anisotropy is used instead. The maximum anisotropy threshold is 0.9.

In February a pixel is classified as water if:

- $s_{0(HH)} < -23$ dB
- OR $s_{0(VV)} < -23$ dB
- OR $PR < -0.02$
- OR $PR_{Max} < -0.02$
- OR Anistropy (max) > 0.9

The Bayesian classification is applied for all ice pixels using the co-location results presented in section 4. To further discriminate ice and open water pixels not correctly classified by the thresholds the mean open water backscatter parameters for wind speeds of 10-15 $m.s^{-1}$ are included as an additional class in the Bayesian classification.

6.1.4 Visualisation

The different parameters are gridded into the EUMETSAT O&SI SAF grid and visualized by automatically scaling the values to a 8-bit grey colour scale. A colour code for the classification results is established giving the following colours to the different ice classes and open water:
Dark green = close multi-year ice,
Light green = close first-year ice,
Red = medium concentration multi-year ice,
Pink = medium concentration first-year ice,
Dark brown = low concentration multi-year ice,
Light brown = low concentration first-year ice, and
Black = open water areas and no data area.

A land mask is not been applied therefore land is misclassified into sea ice. For easier interpretation of the classification results a land mask should be applied.

6.2 Choice of parameters and statistics

The daily standard deviation parameter is dependent on the data type, i.e. spatial and temporal resolution of the gridded product. The reference statistics presented in section 4 is derived from CERSAT data which has a different resolution (25km) than the O&SI SAF data (10km). The daily CERSAT standard deviation is therefore not directly applicable in the O&SI SAF product. Furthermore because of the QS swath width there are not enough measurements at lower latitudes to compute a reliable daily standard deviation. Hence in this example our Bayesian classification is only based on the following parameters: the daily mean HH backscatter, the daily mean VV backscatter and the daily mean polarisation ratio.

Day 42 (February 11th) 2003 is used as an example in this section. The mean monthly QS parameters for the different ice types were merged into seasonal classes: fall (September-November), winter (December-February), spring (March-May) and summer (June-August). The seasonal statistics are presented in the Appendix table C.

6.3 Results on day 42 year 2003

The QS L2B BUFR data February 11th 2003 was used in an operational simulation as described above using the statistics for the different months December, January, February, March and the winter average statistics. The classification was first computed with the non-normalised, then with the normalised Gaussian probability function (see section 5.3).

In general the monthly statistics present important variations. These variations are reflected in the seasonal and monthly classification results respectively. Figure 6.2 shows the difference between the results using (a) the January statistics and (b) the February statistics and the non-normalised Gaussian probability distribution.

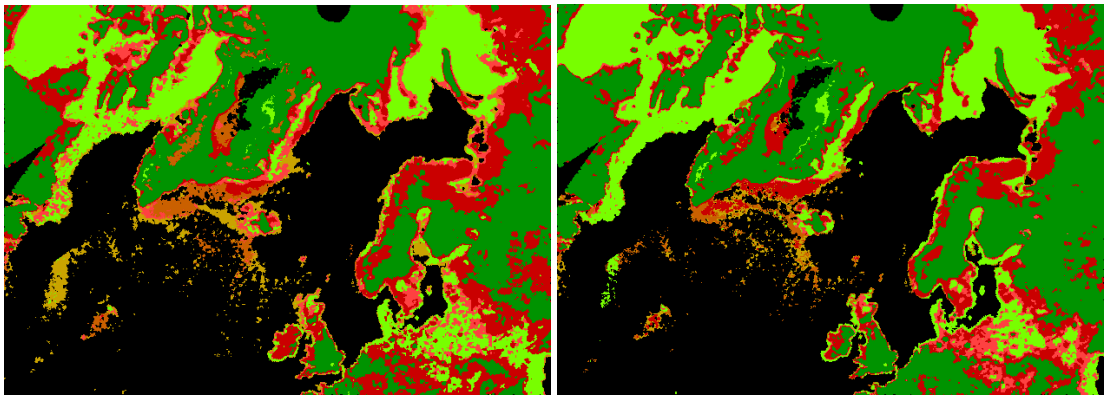

Figure 6.2: Classification results using the non-normalised Gaussian probability distribution and the (a) January and (b) February statistics. Section 6.1.4 describes the colour code.

The choice of statistical average, monthly or seasonal, is significant for the classification result. With QuikScat there is a 2-year monthly record. However this is not climatically representative and we have chosen a seasonal average as an alternative. Figure 6.3 shows the classification results using the winter statistics with the non-normalised Gaussian probability distribution.

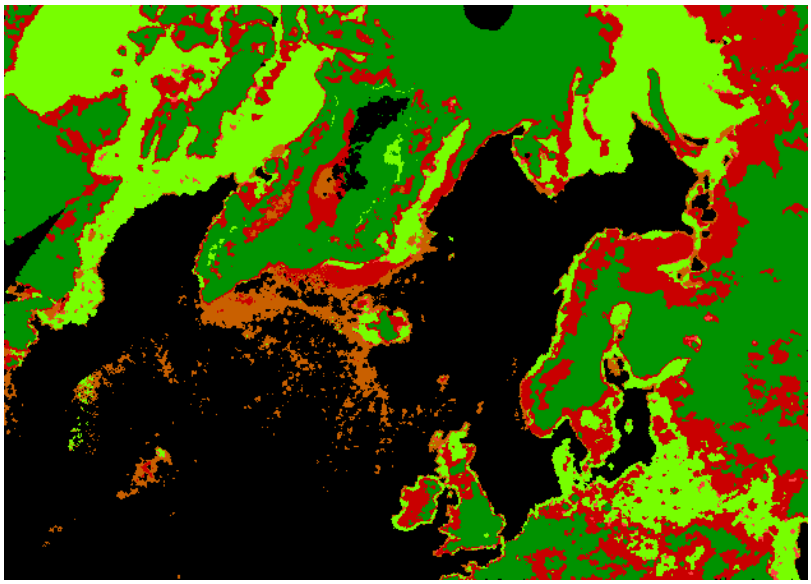

Figure 6.3: Classification result of day 42 2003, using the winter statistics non-normalised Gaussian distribution.

Figure 6.3 shows that with the non-normalised Gaussian distribution. No pixels are classified into medium and open FYI. Figure 6.4 shows the classification using the normalised Gaussian distribution.

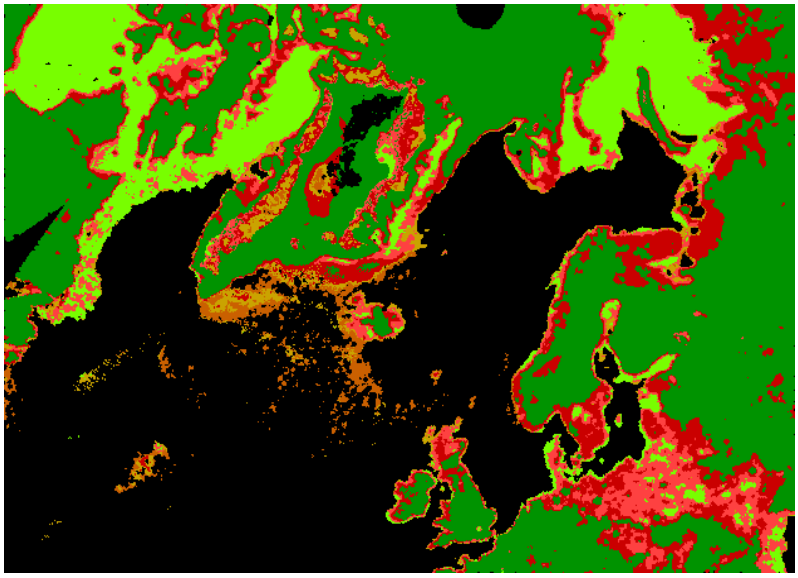

Figure 6.4: Classification result of day 42 2003, using the winter statistics normalised Gaussian distribution.

The classification in figure 6.4 gives satisfying results. There is separation between MYI and FYI. The ice pixels north of Greenland and along the East Greenland coast are classified into MYI and Baffin Bay into FYI. Ocean pixels are however erroneously classified into low concentration classes in areas with high wind speeds. Further high concentration FYI and MYI are misclassified into medium and low concentration ice at the border between MYI and FYI in the Arctic Ocean. At the FYI/MYI border mixtures of high concentration MYI and FYI mimic low concentration backscatter signatures. Comparison with an NOAA AVHRR image in the Barents Sea south of Franz Joseph Land shows that the region which is classified into medium MYI in Figure 6.4 has open leads, the ice concentration estimated from the AVHRR image is however above 70%. Inclusion of the daily standard deviation as an additional classification parameter does reduce misclassifications along the CMY/CFY border, as the example using CERSAT data in section 5 indicated.

7. Discussion

The statistical values for the ice classes necessary for implementation of SeaWinds scatterometer data in the supervised Bayesian classification scheme are presented in this report. Before implementation it is important to discuss and consider some important issues concerning the possibilities and limitations of the data in relation to automated sea ice classification with the given Bayes method. In the following we discuss: 1) the ice charts and the possible error sources, 2) the scatterometer data and the information in relation to ice and water, 3) ice water discrimination the parameters and ambiguities, 4) ice type discrimination and the selection of classes and suitable parameters, and 5) the synergy with radiometer and visual satellite data.

7.1 Greenland ice charts

It is found that, in general the standard deviations on the mean scatterometer parameter signatures are high for each ice chart class. This is not surprising considering the large geographical area and the various meteorological conditions over which the average is found. The differences in backscatter signature between the different ice types, however, indicate that the ice types described in the ice chart can be correlated to the variations in backscatter.

The ice charts define the ice information that is possible to extract using the data background available to the ice analysist. Certain areas like the Baffin Bay (FYI), the Lincoln Sea (MYI) and Wandel Sea (MYI) are well defined with respect to ice type while the ice along the East Coast of Greenland is a mixture of FYI and MYI types. The partial concentrations of the FYI and MYI along the east coast of Greenland are not possible to quantify with the available satellite data. In the ice charts the ice along the East Greenland Coast is only defined as MYI as a consequence of the convention mentioned in section 2.3. Intermediate and low ice concentrations are normally found along the east coast of Greenland and not in the Central Arctic. Therefore this assumption concerning MYI will give the largest error for intermediate and low concentration MYI.

Several ice chart classes are merged in order to create more general classes. All new-ice, young-ice and first-year ice were combined to define the FYI class. Even though the charts are ordered seasonally FYI is usually a combination of different types. FYI is in the ice chart exclusively defined for Baffin Bay.

In spite of these short-comings the ice charts represent all ice types around Greenland and most Arctic ice types as well.

7.2 SeaWinds scatterometer data

The near-real-time LB2 SeaWinds swath data are used in the co-location to generate typical signatures for different ice types. We use swath data in order to collect enough measurements for computing meaningful statistical mean and variance. Mean signatures for the different ice chart classes are computed by averaging all co-located backscatter measurements and ice chart data points. This average and its variability describes the backscatter variations for a given ice chart class around Greenland. The ice chart defines ice type, concentration etc. which are important parameters for backscattering, but parameters

such as ice temperature, surface roughness, snow cover etc. which are not defined in the ice chart also play an important role for the backscattering (Nghiem et al., 1995; Onstott, 1991). The latter parameters are likely to be different for the sea ice over the vast area that the ice chart is covering. Part of the ice class backscatter variance is due to these physical differences. The normalised daily standard deviation is a measure of the backscatter variability within a pixel during one day. Intermediate and low ice concentrations have a higher standard deviation than high ice concentrations. The contrast in backscatter between calm open water and ice is high. If both ice and open water is found within a grid pixel during a day the variability is high. Further open water areas influenced by surface winds within the intermediate and low concentration ice may give anisotropic backscatter and thereby contribute to the higher variability for these ice concentrations compared to high ice concentration areas.

7.3 Ice-open water discrimination

Two SeaWinds parameters can be computed which emphasise the physical differences between the backscattering from open water and sea ice. These are the 1) anisotropy defined as the difference over the sum of fore and aft backscatter measurements, and 2) the polarisation ratio defined as the difference over the sum of backscatter measurements at the two SeaWinds channels HH and VV.

These two parameters makes effective separation between ice and open water even under conditions where the backscatter contrast is small e.g. ice surface melting, medium high surface wind speeds (<15m/s).

The standard deviation of the backscatter is also an effective ice-water discrimination parameter. It is computed when the swath data are gridded in maps for a given period and resolution. CERSAT is issuing daily gridded backscatter maps with 25 km pixel resolution. These maps are used to compute the standard deviation for the different ice chart classes. The normalised standard deviation of the backscatter describe 3 types of variability: 1) the variability due to the anisotropic backscattering of the ocean surface, 2) the daily backscatter variability due to changing geophysical conditions, and 3) instrumental and processing noise.

7.4 Ice type discrimination

FYI and MYI have different scattering properties. MYI (~-9dB) has much higher backscatter than FYI (~-16dB) and the polarisation ratio mean is higher for FYI (~0.23) than MYI (~0.17). Both the backscatter and the polarisation ratio are related to the ice concentration and it is therefore important to define separate ice classes with respect to concentration and ice type. We define in section 2.5 6 classes, 3 concentrations and 2 ice types. During the classification trials in section 5.2 it is found that classification results are improved by including the normalised standard deviation. The normalised standard deviation is not related to ice type but ice concentration. Anyway it improves the ice type classification result if it is included. The inclusion of standard deviation in the classification is illustrating the importance of both discriminating between concentration and types to make a proper classification. Similar or even better classification results may also be possible by including parameters from other sensors e.g. radiometer ice concentration. The

radiometer ice concentration may have a similar function as the standard deviation in the classification but it is less ‘noisy’.

7.5 Synergy with other satellite data

The O&SI SAF ice product is a fusion of information from different sensors i.e. DMSP-SSM/I, NOAA-AVHRR and scatterometer. QS is well suited for ice type discrimination and ice - water discrimination. The AVHRR data are used for ice – water discrimination and SSM/I for ice type, ice concentration and ice water discrimination. By combining parameters from different sensors each of these products may possibly be improved. However only parameters with meaningful information for a particular task should be included. The synergy of the different satellite sensors is not studied in this report, but should be considered in the future.

8. Conclusions

The results in section 5.2 and 6.3 show that QS data are useful for sea ice classification during the cold season (September-May). This lets us conclude that all defined parameters i.e. HH, VV, polarisation ratio and daily standard deviation of the backscatter are useful for ice type classification. However, statistics for the daily standard deviation is still to be established for the L2B data set. By visual inspection both the ice edge and the ice types match well coincident ice charts. The backscatter separation is most effective for high ice concentrations (>70%), but the mean backscatter derived parameters are also separated for intermediate concentrations (30-70%). Ice types can not be separated for low ice concentrations (<30%) and these classes also overlap ocean backscatter parameters at high wind speeds (>15m/s). Therefore the two low concentration classes (FYI and MYI < 30%) can be merged. In summer (June-August) it is impossible to discriminate ice types because of ice surface melt. However separation between ice and water is still possible during summer.

Separation between ice and water is done using the QS parameters i.e. standard deviation of the backscatter and polarisation ratio, which are distinct for ice and water. Ice type classification is done similarly using parameters with separation between different ice classes i.e. HH, VV, polarisation ratio and standard deviation of the backscatter. Inclusion of open water statistics in the Bayesian classification eliminates some of the misclassified ocean pixels. It is at the same time possible that low concentration ice pixels are misclassified into ocean pixels.

The best ice type classification results are achieved by normalising the Gaussian density function for each ice class to 1 before computing the probability and combining these with the Bayes formulae. Without normalisation differences between standard deviation erroneously dominate the ice type classification.

NIC is currently using a resolution enhanced QS product (Long et al., 1993; Long, 2000) in the operational service. This product would comply well with the 10km grid currently used in O&SI SAF. However, this product is more ‘noisy’ than a daily product and some of the enhanced resolution is annihilated by the 36hour ice dynamics.

The computed statistics cover the entire Greenland region and the ice class signatures have a high standard deviation. Sub-dividing the ice chart into regions before computing the statistical parameters may reduce the standard deviation and in terms of backscatter signature create better defined classes. The ice class signatures are during the processing tested for being Gaussian using a Kolmogorov-Smirnov test. Most of the class signatures are not Gaussian. Visual inspection of the distributions indicates that an important reason for the data not being Gaussian is because the data are multi-modal.

The supervised Baysian classifications scheme which is used in the current O&SI SAF ice product is assuming equal initial probabilities for both ice - water and different ice types. Climatology i.e. past years ice conditions is additional information that should be included in the ice classification. For example it is well know that Baffin Bay is almost exclusively covered by FYI except for the very small quantities of MYI that drift through Narres Strait. Lincoln Sea and Wandel Sea are dominated by MYI and certain water areas are ice free all

year round. The climatology could for example be based on a reprocessed O&SI SAF ice products with SSM/I radiometer and ERS scatterometer data from 1992-2001.

Backscatter parameters are very sensitive to wind over open water and the backscatter is sensitive to ice surface melt. Other ‘meteorological’ parameters such as snow cover and ice temperature also influence the backscatter. HIRLAM the local area numerical models which are operated both at DMI and MET.NO compute meteorological parameters which are important for the backscatter signatures both over water and ice. The predictions of this model could guide the ice classification by selecting proper statistics for a given meteorological situation and thereby improve the classification.

9. References

Johannesen, O. M., Shalina, E. V., Miles, M. W. (1999): Satellite evidence for an Arctic sea ice cover in transformation. *Science, 286(5446), pp. 1937-1939.*

Leidner, S. M., R. N. Hoffman and J. Augenbaum (2000): SeaWinds scatterometer real-time bufr geophysical data product, users guide, version 2.3.0.

Long, D.G. (2000): Standard BYU QuikScat/Seawinds land/ice image products. QuikScat Image Product documentation, http://www.scp.byu.edu/docs/pdf/QscatReport3.pdf .

Long, D.G. and Drinkwater, M.R. (1999): Cryosphere application of NSCAT data. *IEEE Trans. Geosci. Remote Sensing*, 37(3), 1671-1684.

Long, D.G., Hardin, P.J., and Whiting, P.T. (1993): Resolution enhancement of spaceborne scatterometer data. *IEEE Trans. Geosci. Remote Sensing*, 31(3), 700-715.

Lungu, T. (ed.) (2001): NASA Quick Scatterometer - QuikSCAT science data product user's manual: Overview and geophysical data products. Version 2.2, JPL-report D-18053, Jet Propulsion Laboratory, California Institute of Technology, Pasadena, CA.

Nghiem, S.V., Kwok, R., Yueh, S.H., Drinkwater, M.R. (1995): Polarimetric signatures of sea ice – 1. Theoretical models. J. Geophys. Res., 100(C7), 13,665-13,679.

Nghiem, S. V., R. Kwok, S. H. Yueh, and M. R. Drinkwater (1995): Polarimetric signatures of sea ice. 2. Experimental observations, J. Geophys. Res., Vol. 100, No. C7, pp. 13681-13698.

Onstott, R. G. (1991): SAR and scatterometer signatures of sea ice. In: Microwave remote sensing of sea ice, Ed.: Carsey, Geophysical monograph 68, American Geophysical Union.

Remund, Q.P. and Long, D.G. (1998): Sea ice mapping algorithm for QuikScat and Seawinds. *Proceeding of the 1998 IEEE International Geoscience and Remote Sensing Symposium*, Seattle, WA, July 1998.

Remund, Q.P. and Long, D.G. (1999): Sea ice extent mapping using Ku-band scatterometer data. *J. Geophys. Res.*, 104(C5), 11,515-11,527.

Tonboe, R. (2001): QuikSCAT – SeaWinds scatterometer observations of sea ice types around Greenland. *Proceedings of SPIE 2001 8th international symposium on remote sensing, Toulouse, France.*

Tonboe, R. and Ezraty, R. (2002): Monitoring of new-ice in Greenland waters. *Proceeding of the 1998 IEEE International Geoscience and Remote Sensing Symposium*, Toronto, Canada, June 2002.

Wentz, F. J. and D. K. Smith (1999): A model function for the ocean-normalised radar cross section at 14GHz derived from NSCAT observations, Journal of Geophysical Research, Vol. 104, No. C5, pp. 11499-11514.

10. Appendix

Table A1: 4 class statistical values: close first year ice and close multi year ice (ice concentration >70%)

	TYPE	N	HH	HH	HH	VV	VV	VV	POL	POL	HH-std	HH-std	VV-std	VV-std
			MEAN	dB	std	MEAN	dB	std	MEAN	std	norm	std	norm	std
Oct.	CFY	418	0.05283	-12.77119	0.02400	0.03962	-14.02129	0.01615	0.13288	0.10126				
Nov.	CFY	549	0.04139	-13.83126	0.02098	0.02907	-15.36615	0.01478	0.17587	0.06979				
Dec.	CFY	2642	0.05472	-12.61878	0.04548	0.03176	-14.98174	0.02351	0.24803	0.06904	0.16318	0.05229	0.15930	0.05164
Jan.	CFY	5619	0.04416	-13.54941	0.02564	0.02664	-15.74401	0.01486	0.24296	0.06391	0.16280	0.05350	0.15968	0.05124
Feb.	CFY	7043	0.03812	-14.18893	0.01854	0.02427	-16.14912	0.01278	0.22848	0.07018	0.15281	0.04250	0.15233	0.04514
Mar.	CFY	8909	0.03182	-14.97245	0.01426	0.02000	-16.98883	0.00984	0.23390	0.05759	0.15166	0.04590	0.15162	0.04705
Apr.	CFY	6120	0.02804	-15.52299	0.01161	0.01755	-17.55723	0.00786	0.23319	0.06288	0.15304	0.05423	0.15785	0.06040
May	CFY	5195	0.03393	-14.69480	0.02387	0.02192	-16.59159	0.01474	0.22567	0.07016	0.17244	0.07568	0.17150	0.06960
Jun.	CFY	9024	0.04439	-13.52734	0.03213	0.02724	-15.64793	0.01862	0.20780	0.11964	0.31513	0.11351	0.29366	0.10433
Jul.	CFY	3073	0.02693	-15.69699	0.02199	0.01629	-17.87972	0.01260	0.22335	0.10424	0.25904	0.11467	0.25059	0.09907
Aug.	CFY	182	0.01226	-19.11510	0.01819	0.00837	-20.77534	0.01074	0.08019	0.24862				
Sep.	CFY	3	0.03189	-14.96291	0.02860	0.02323	-16.34044	0.02073	0.10428	0.09049				
Oct.	CMY	7447	0.13407	-8.72672	0.06248	0.09561	-10.19497	0.04587	0.17156	0.05439	0.14001	0.04892	0.13621	0.05113
Nov.	CMY	8183	0.13806	-8.59938	0.05521	0.09916	-10.03672	0.04129	0.17720	0.09579	0.13508	0.04803	0.13130	0.05087
Dec.	CMY	9981	0.13700	-8.63273	0.05470	0.09461	-10.24081	0.03786	0.18923	0.08751	0.15410	0.07089	0.14710	0.06975
Jan.	CMY	9357	0.11962	-9.22193	0.04628	0.08425	-10.74415	0.03313	0.17337	0.05566	0.14675	0.06248	0.13919	0.05903
Feb.	CMY	7999	0.11457	-9.40933	0.05010	0.08184	-10.87018	0.03602	0.17134	0.07684	0.13376	0.04963	0.12659	0.04096
Mar.	CMY	13059	0.10692	-9.70925	0.04826	0.07693	-11.13904	0.03513	0.16660	0.06324	0.13761	0.04990	0.13309	0.04893
Apr.	CMY	8028	0.09717	-10.12481	0.05176	0.06873	-11.62873	0.03747	0.17698	0.05749	0.15433	0.08434	0.15127	0.08328
May	CMY	9364	0.09234	-10.34605	0.05383	0.06415	-11.92830	0.03780	0.18550	0.07743	0.17750	0.08868	0.16982	0.08612
Jun.	CMY	17622	0.03797	-14.20537	0.03185	0.02558	-15.92049	0.02207	0.20160	0.09416	0.24530	0.12080	0.24931	0.11669
Jul.	CMY	7121	0.02997	-15.23357	0.01654	0.02051	-16.88013	0.01064	0.19618	0.14113	0.22563	0.09536	0.23630	0.09172
Aug.	CMY	2825	0.06944	-11.58409	0.06196	0.04720	-13.26067	0.04287	0.20140	0.10172	0.20192	0.09788	0.22663	0.10493
Sep.	CMY	3363	0.17494	-7.57106	0.06846	0.12133	-9.16028	0.04754	0.17711	0.05912	0.15042	0.09220	0.14484	0.09858

Table A2: 4 class statistical values: open first year ice and open multi year ice (ice concentration <70%)

	TYPE	N	HH	HH	HH	VV	VV	VV	POL	POL	HH-std	HH-std	VV-std	VV-std
			MEAN	dB	std	MEAN	dB	std	MEAN	std	norm	std	norm	std
Oct.	LFY	409	0.03833	-14.16450	0.01952	0.02904	-15.37018	0.01345	0.12283	0.12286	0.20440	0.07292	0.18888	0.06369
Nov.	LFY	1457	0.04409	-13.55670	0.01728	0.03194	-14.95665	0.01266	0.15779	0.09544	0.20888	0.08436	0.23029	0.09945
Dec.	LFY	2001	0.04778	-13.20772	0.02845	0.03376	-14.71662	0.01894	0.16204	0.13352	0.23970	0.09664	0.21360	0.09510
Jan.	LFY	885	0.04587	-13.38500	0.01880	0.03358	-14.73958	0.01269	0.14233	0.10501	0.18566	0.07247	0.19087	0.05811
Feb.	LFY	976	0.04877	-13.11865	0.02038	0.03674	-14.34908	0.01488	0.15985	0.18223	0.17881	0.06524	0.16962	0.07648
Mar.	LFY	1022	0.04208	-13.75904	0.01870	0.03296	-14.82066	0.01415	0.13161	0.17683	0.19473	0.09044	0.18383	0.06263
Apr.	LFY	326	0.02645	-15.77509	0.01489	0.01988	-17.01518	0.01013	0.13701	0.14482	0.20092	0.09919	0.20626	0.08524
May	LFY	869	0.03387	-14.70134	0.02096	0.02462	-16.08659	0.01470	0.17380	0.19766	0.25721	0.10413	0.25853	0.09652
Jun.	LFY	403	0.03055	-15.15017	0.02482	0.01902	-17.20904	0.01460	0.20955	0.10805	0.18267	0.16591	0.17800	0.15470
Jul.	LFY	863	0.00938	-20.27705	0.01127	0.00702	-21.53849	0.00685	0.10923	0.18073				
Aug.	LFY	225	0.00627	-22.03010	0.00678	0.00423	-23.73660	0.00424	0.15708	0.15866				
Sep.	LFY	9	0.04533	-13.43653	0.02197	0.02807	-15.51742	0.01422	0.21124	0.08243				
Oct.	LMY	1548	0.04572	-13.39903	0.03094	0.03451	-14.62055	0.02221	0.13216	0.10263	0.21756	0.08286	0.20498	0.07949
Nov.	LMY	880	0.06153	-12.10913	0.02667	0.04297	-13.66814	0.01947	0.17494	0.06772	0.17576	0.08986	0.17056	0.08648
Dec.	LMY	362	0.05049	-12.96812	0.02515	0.03631	-14.40022	0.01550	0.14787	0.10802	0.26950	0.12850	0.24860	0.11890
Jan.	LMY	623	0.07373	-11.32362	0.03110	0.05289	-12.76594	0.02094	0.15416	0.07913	0.23198	0.09653	0.23544	0.09248
Feb.	LMY	369	0.06288	-12.01501	0.02667	0.04842	-13.15011	0.01781	0.11341	0.09339	0.20480	0.09395	0.19389	0.11349
Mar.	LMY	520	0.05162	-12.87148	0.02186	0.03952	-14.03183	0.01473	0.12627	0.12093	0.18304	0.06789	0.18907	0.06844
Apr.	LMY	351	0.05299	-12.75814	0.02347	0.04078	-13.89606	0.01723	0.11623	0.09615	0.18394	0.06689	0.18052	0.06394
May	LMY	572	0.05456	-12.63134	0.02794	0.03784	-14.22095	0.01762	0.17396	0.11699	0.28392	0.10633	0.26055	0.09946
Jun.	LMY	3646	0.02024	-16.93854	0.01417	0.01467	-18.33688	0.00930	0.14703	0.13796	0.27730	0.11517	0.26034	0.09877
Jul.	LMY	6488	0.00969	-20.13631	0.00836	0.00774	-21.11091	0.00606	0.10562	0.17395	0.28546	0.12762	0.23927	0.12308
Aug.	LMY	4684	0.00936	-20.28631	0.01232	0.00705	-21.51626	0.00837	0.11052	0.18064	0.23448	0.09379	0.30971	0.14181
Sep.	LMY	2362	0.03445	-14.62811	0.03806	0.02614	-15.82777	0.02605	0.08976	0.19196	0.23889	0.10134	0.23909	0.10822

Table B1: 6-class statistical values: close multi-year ice and close first-year ice (ice concentration >70%)

	TYPE	N	HH	HH	HH	VV	VV	VV	POL	POL	HH-std	HH-std	VV-std	VV-std
			MEAN	dB	std	MEAN	dB	std	MEAN	std	norm	std	norm	std
Oct.	CMY	7447	0.13407	-8.72672	0.06248	0.09561	-10.19497	0.04587	0.17156	0.05439				
Nov.	CMY	8183	0.13806	-8.59938	0.05521	0.09916	-10.03672	0.04129	0.17720	0.09579	0.13508	0.04803	0.13130	0.05087
Dec.	CMY	9981	0.13700	-8.63273	0.05470	0.09461	-10.24081	0.03786	0.18923	0.08751	0.15408	0.07090	0.14710	0.06975
Jan.	CMY	9357	0.11962	-9.22193	0.04628	0.08425	-10.74415	0.03313	0.17337	0.05566	0.14675	0.06248	0.13919	0.05903
Feb.	CMY	7999	0.11457	-9.40933	0.05010	0.08184	-10.87018	0.03602	0.17134	0.07684	0.13376	0.04963	0.12659	0.04096
Mar.	CMY	13059	0.10692	-9.70925	0.04826	0.07693	-11.13904	0.03513	0.16660	0.06324	0.13761	0.04990	0.13309	0.04893
Apr.	CMY	8028	0.09717	-10.12481	0.05176	0.06873	-11.62873	0.03747	0.17698	0.05749	0.15433	0.08434	0.15127	0.08328
May	CMY	9364	0.09234	-10.34605	0.05383	0.06415	-11.92830	0.03780	0.18550	0.07743	0.17750	0.08868	0.16982	0.08612
Jun.	CMY	17622	0.03797	-14.20537	0.03185	0.02558	-15.92049	0.02207	0.20160	0.09416	0.24530	0.12080	0.24931	0.11669
Jul.	CMY	7121	0.03000	-15.22927	0.01654	0.02051	-16.88013	0.01064	0.19618	0.14113	0.22563	0.09536	0.23630	0.09172
Aug.	CMY	2825	0.06944	-11.58409	0.06196	0.04720	-13.26067	0.04287	0.20140	0.10172	0.20192	0.09788	0.22663	0.10493
Sep.	CMY	3363	0.17494	-7.57106	0.06846	0.12133	-9.16028	0.04754	0.17711	0.05912	0.15042	0.09220	0.14484	0.09858
Oct.	CFY	418	0.05283	-12.77119	0.02400	0.03962	-14.02129	0.01615	0.13288	0.10126				
Nov.	CFY	549	0.04139	-13.83126	0.02098	0.02907	-15.36615	0.01478	0.17587	0.06979				
Dec.	CFY	2642	0.05472	-12.61878	0.04548	0.03176	-14.98174	0.02351	0.24803	0.06904	0.16318	0.05229	0.15929	0.05164
Jan.	CFY	5619	0.04416	-13.54941	0.02564	0.02664	-15.74401	0.01486	0.24296	0.06391	0.16280	0.05350	0.15968	0.05124
Feb.	CFY	7043	0.03812	-14.18893	0.01854	0.02427	-16.14912	0.01278	0.22848	0.07018	0.15281	0.04250	0.15233	0.04514
Mar.	CFY	8909	0.03182	-14.97245	0.01426	0.02000	-16.98883	0.09836	0.23390	0.05759	0.15166	0.04590	0.15162	0.04705
Apr.	CFY	6120	0.02804	-15.52299	0.01161	0.01755	-17.55723	0.07858	0.23332	0.06288	0.15304	0.05423	0.15785	0.06040
May	CFY	5195	0.03393	-14.69480	0.02387	0.02129	-16.71784	0.01474	0.22567	0.07016	0.17244	0.07568	0.17150	0.06960
Jun.	CFY	9024	0.04439	-13.52734	0.03213	0.02724	-15.64793	0.01862	0.20780	0.11964	0.31513	0.11351	0.29366	0.10433
Jul.	CFY	3073	0.02693	-15.69699	0.02199	0.01629	-17.87972	0.01260	0.22335	0.10424	0.25904	0.11467	0.25059	0.09907
Aug.	CFY	182	0.01226	-19.11510	0.01819	0.00837	-20.77534	0.01074	0.08019	0.24862				
Sep.	CFY	3	0.03189	-14.96291	0.02860	0.02323	-16.34044	0.02073	0.10428	0.09049				

Table B2: 6 class statistical values: medium multi-year ice and medium first-year ice (30% < ice concentration <70%)

	TYPE	N	HH	HH	HH	VV	VV	VV	POL	POL	HH-std	HH-std	VV-std	VV-std
			MEAN	dB	std	MEAN	dB	std	MEAN	std	norm	std	norm	std
Oct.	MMY	1446	0.04670	-13.30730	0.03107	0.03474	-14.59183	0.02254	0.14418	0.08775	0.21797	0.08321	0.20577	0.07991
Nov.	MMY	839	0.06239	-12.04920	0.02591	0.04349	-13.61661	0.01901	0.17694	0.06663	0.17341	0.09071	0.16759	0.08680
Dec.	MMY	289	0.05271	-12.78074	0.02582	0.03648	-14.37957	0.01573	0.16930	0.09539	0.26383	0.12735	0.24629	0.12068
Jan.	MMY	603	0.07436	-11.28672	0.03105	0.05312	-12.74750	0.02091	0.15685	0.07811	0.22988	0.09429	0.23494	0.09274
Feb.	MMY	348	0.06367	-11.96072	0.02676	0.04909	-13.08998	0.01773	0.11259	0.09209	0.20480	0.09395	0.19389	0.11349
Mar.	MMY	455	0.05018	-12.99461	0.02130	0.03839	-14.15782	0.01454	0.12781	0.12452	0.17554	0.05503	0.18650	0.06809
Apr.	MMY	345	0.05351	-12.71589	0.02331	0.04111	-13.86063	0.01717	0.11791	0.09549	0.18394	0.06689	0.18052	0.06394
May	MMY	517	0.05613	-12.50797	0.02749	0.03863	-14.13042	0.01720	0.17909	0.11007	0.28940	0.10805	0.26533	0.10139
Jun.	MMY	3141	0.02131	-16.71518	0.01416	0.01527	-18.16246	0.00924	0.15576	0.12607	0.27260	0.11575	0.25552	0.09611
Jul.	MMY	5128	0.01050	-19.78935	0.00841	0.00811	-20.91193	0.00595	0.12603	0.15449	0.26867	0.11741	0.21200	0.09784
Aug.	MMY	4070	0.00979	-20.09084	0.01291	0.00728	-21.37630	0.00873	0.11853	0.17709	0.22965	0.09677	0.30012	0.14240
Sep.	MMY	2039	0.03701	-14.31646	0.03883	0.02770	-15.57583	0.02671	0.10425	0.17204	0.23865	0.10217	0.23827	0.10934
Oct.	MFY	362	0.04044	-13.93189	0.01932	0.02996	-15.23487	0.01363	0.14232	0.10516	0.20440	0.07292	0.18888	0.06369
Nov.	MFY	1309	0.04565	-13.40588	0.01704	0.03289	-14.82910	0.01258	0.16162	0.09419	0.21190	0.08400	0.23234	0.09978
Dec.	MFY	1470	0.04756	-13.22795	0.02786	0.03299	-14.81578	0.01871	0.17567	0.13539	0.23411	0.08938	0.20295	0.08514
Jan.	MFY	794	0.04774	-13.21099	0.01825	0.03439	-14.63530	0.01263	0.15493	0.09369	0.18566	0.07247	0.19087	0.05811
Feb.	MFY	830	0.04861	-13.13292	0.01882	0.03530	-14.52287	0.01329	0.18215	0.18286	0.17881	0.06524	0.16962	0.07648
Mar.	MFY	829	0.04261	-13.70529	0.01680	0.03192	-14.95978	0.01211	0.16262	0.17087	0.19382	0.09110	0.18257	0.06244
Apr.	MFY	185	0.02856	-15.44303	0.01437	0.02095	-16.78878	0.00937	0.14783	0.09973	0.19500	0.09500	0.21213	0.09487
May	MFY	594	0.03971	-14.01100	0.02140	0.02756	-15.59721	0.01432	0.21357	0.20261	0.25400	0.10800	0.25205	0.10255
Jun.	MFY	373	0.03096	-15.09185	0.02468	0.01927	-17.15141	0.01463	0.21206	0.10701	0.18267	0.16591	0.17800	0.15470
Jul.	MFY	694	0.01028	-19.88134	0.01191	0.00723	-21.41162	0.00690	0.13061	0.15497				
Aug.	MFY	216	0.00614	-22.11619	0.00682	0.00410	-23.87004	0.00422	0.15804	0.16073				
Sep.	MFY	9	0.04533	-13.43653	0.02197	0.02807	-15.51742	0.01422	0.21112	0.08243				

Table B3: 6 class statistical values: open multi-year ice and open first-year ice (ice concentration <30%)

	TYPE	N	HH	HH	HH	VV	VV	VV	POL	POL	HH-std	HH-std	VV-std	VV-std
			MEAN	dB	std	MEAN	dB	std	MEAN	std	norm	std	norm	std
Oct.	OMY	102	0.03154	-15.01111	0.02557	0.03098	-15.08989	0.01688	-0.03933	0.13982	0.14467	0.13683	0.11800	0.10259
Nov.	OMY	41	0.04156	-13.81377	0.03461	0.03063	-15.13881	0.02476	0.13050	0.07997	0.19733	0.08753	0.20400	0.08962
Dec.	OMY	73	0.04108	-13.86370	0.02074	0.03508	-14.54990	0.01522	0.06244	0.11412	0.28970	0.14990	0.25490	0.12218
Jan.	OMY	20	0.05211	-12.83112	0.02944	0.04421	-13.54440	0.02349	0.06490	0.06562				
Feb.	OMY	21	0.04805	-13.18289	0.02407	0.03608	-14.42782	0.01743	0.11757	0.11658				
Mar.	OMY	65	0.06072	-12.16661	0.02445	0.04673	-13.30376	0.01488	0.11160	0.09152	0.22267	0.15466	0.18400	0.11348
Apr.	OMY	6	0.02056	-16.86956	0.01310	0.01861	-17.30300	0.01148	0.02871	0.08632				
May	OMY	55	0.03802	-14.19976	0.02737	0.02880	-15.40653	0.01905	0.12384	0.16314	0.21400	0.11510	0.19400	0.10504
Jun.	OMY	505	0.01356	-18.67612	0.01229	0.01091	-19.62135	0.00884	0.09213	0.18745	0.26429	0.13253	0.25171	0.14714
Jul.	OMY	1360	0.00665	-21.77505	0.00742	0.00637	-21.96202	0.00626	0.02866	0.21653	0.11100	0.15698	0.11200	0.15839
Aug.	OMY	614	0.00644	-21.91047	0.00648	0.00548	-22.61378	0.00505	0.05727	0.19457	0.21900	0.15442	0.30250	0.22955
Sep.	OMY	323	0.01819	-17.40072	0.02784	0.01596	-17.96858	0.01841	-0.00245	0.27014	0.09000	0.12728	0.10700	0.15132
Oct.	OFY	47	0.02133	-16.71091	0.01232	0.02149	-16.67844	0.00993	-0.03228	0.13985				
Nov.	OFY	148	0.03012	-15.21159	0.01296	0.02341	-16.30524	0.01021	0.12227	0.10000				
Dec.	OFY	531	0.04832	-13.15882	0.03011	0.03579	-14.46250	0.01947	0.12399	0.12061	0.22450	0.13420	0.21270	0.13230
Jan.	OFY	91	0.02902	-15.37362	0.01556	0.02612	-15.82994	0.01119	0.03037	0.13076				
Feb.	OFY	146	0.04948	-13.05535	0.02796	0.04452	-13.51455	0.02011	0.03162	0.11316				
Mar.	OFY	193	0.03963	-14.01976	0.02536	0.03713	-14.30252	0.02023	-0.00204	0.13546	0.11900	0.16829	0.10900	0.15415
Apr.	OFY	141	0.02355	-16.28028	0.01528	0.01836	-17.36175	0.01103	0.12136	0.18793	0.15350	0.07382	0.14686	0.06918
May	OFY	275	0.02125	-16.72559	0.01293	0.01854	-17.32007	0.01356	0.09031	0.14848	0.23964	0.11945	0.25909	0.10876
Jun.	OFY	30	0.02515	-15.99531	0.02666	0.01571	-18.03907	0.01413	0.16840	0.11979				
Jul.	OFY	169	0.00566	-22.47414	0.00703	0.00612	-22.13391	0.00660	0.02002	0.24210				
Aug.	OFY	9	0.00876	-20.57397	0.00577	0.00701	-21.54406	0.00433	0.10792	0.10033				
Sep.	OFY	0												

Table C: 6 class statistical values averaged over each season: winter (December-February), spring (March-May), summer (June-August) and autumn (September-November)

Season	Ice class	HH	HH	VV	VV	POL	POL	HH-std	HH-std	VV-std	VV-std
		MEAN	std	MEAN	std	MEAN	std	norm	std	norm	std
winter	CMY	0.124489	0.050469	0.087328	0.035703	0.178566	0.073488	0.145624	0.061792	0.138393	0.057656
winter	CFY	0.043202	0.025798	0.026434	0.015396	0.237171	0.067682	0.158271	0.048229	0.156226	0.0485
winter	MMY	0.066314	0.028628	0.04811	0.018811	0.147329	0.086058	0.230752	0.101901	0.226061	0.105073
winter	MFY	0.047886	0.022969	0.03397	0.015696	0.172085	0.137423	0.206837	0.078562	0.190905	0.075881
winter	OMY	0.044299	0.022882	0.036863	0.017076	0.073029	0.106064	0	99999999	0	99999999
winter	OFY	0.046253	0.027978	0.036303	0.01861	0.095336	0.120393	0	99999999	0	99999999
winter	15 m/s windover ocean	0.005012	0.03	0.005012	0.03	-0.03	0.130762	0	99999999	0	99999999
spring	CMY	0.099867	0.050898	0.070836	0.036569	0.175149	0.066085	0.154281	0.070906	0.149178	0.069422
spring	CFY	0.031217	0.015928	0.019592	0.070895	0.23161	0.062423	0.157414	0.05607	0.158611	0.05688
spring	MMY	0.053388	0.024259	0.039198	0.016273	0.145345	0.111243	0.222437	0.078951	0.215879	0.080074
spring	MFY	0.03992	0.01822	0.029045	0.012612	0.179742	0.174407	0.216188	0.09779	0.211635	0.080987
spring	OMY	0.0489	0.025185	0.037565	0.016539	0.112996	0.122533	0	99999999	0	99999999
spring	OFY	0.027609	0.017413	0.024388	0.01509	0.06823	0.153485	0.181462	0.124364	0.18554	0.113982
spring	15 m/s windover ocean	0.005012	0.03	0.005012	0.03	-0.03	0.130762	0	99999999	0	99999999
summer	CMY	0.039136	0.030979	0.026488	0.021251	0.200177	0.107065	0.235771	0.111878	0.243623	0.109033
summer	CFY	0.039544	0.029382	0.024221	0.016995	0.209801	0.1177	0	99999999	0	99999999
summer	MMY	0.013016	0.011361	0.009658	0.007703	0.131123	0.154709	0.256797	0.110177	0.252143	0.112094
summer	MFY	0.015594	0.014766	0.010201	0.008695	0.158906	0.141995	0	99999999	0	99999999
summer	OMY	0.008004	0.008176	0.007071	0.006486	0.048675	0.205164	0.168976	0.151365	0.187644	0.173723
summer	OFY	0.008602	0.009804	0.00754	0.007587	0.045226	0.218327	0	99999999	0	99999999
summer	15 m/s windover ocean	0.005012	0.03	0.005012	0.03	-0.03	0.130762	0	99999999	0	99999999
autumn	CMY	0.143025	0.060404	0.101693	0.044191	0.174972	0.073063	0	99999999	0	99999999
autumn	CFY	0.046289	0.022301	0.033594	0.015387	0.157126	0.083417	0	99999999	0	99999999
autumn	MMY	0.045174	0.033725	0.033115	0.023822	0.131709	0.1234	0.219072	0.093608	0.213684	0.095122
autumn	MFY	0.044523	0.017555	0.032234	0.012815	0.157723	0.096492	0	99999999	0	99999999
autumn	OMY	0.023171	0.027936	0.02054	0.018637	0.001174	0.224883	0	99999999	0	99999999
autumn	OFY	0.028	0.012804	0.022949	0.010138	0.085016	0.109601	0	99999999	0	99999999
autumn	15 m/s windover ocean	0.005012	0.03	0.005012	0.03	-0.03	0.130762	0	99999999	0	99999999